CRYSTAL GROWTH & DESIGN

pubs.acs.org/crystal

Review

# (111) Faceted Metal Oxides: A Review of Synthetic Methods

Raiven I. Balderas, Cristian V. Ciobanu, and Ryan M. Richards*

Cite This: *Cryst. Growth Des.* 2022, 22, 6296–6322

Read Online

ACCESS | Metrics & More | Article Recommendations

**ABSTRACT:** Material design and synthesis have made tremendous impacts in the scientific community by unleashing a material's true potential via enhanced properties and applications. Over the years, advanced synthetic strategies have emerged and have been expanded to not only control the size and shape of nanoparticles but also to control the preferential growth of surface facets, paving the way for new materials with facet-dependent properties. Metal oxide (111) facets as compared to their potentially more stable counterpart facets (e.g., (100), (110)) have recently exhibited enriched chemical properties owing to their unique surface arrangement. As a result, metal oxide (111) faceted surfaces have been used in applications such as catalysis, sorbents, batteries, etc. This review aims to provide a perspective on the synthetic processes utilized to expose (111) surfaces and the governing factors/synthetic parameters that expose them across various metal oxides of different crystal structures as well as some of their applications.

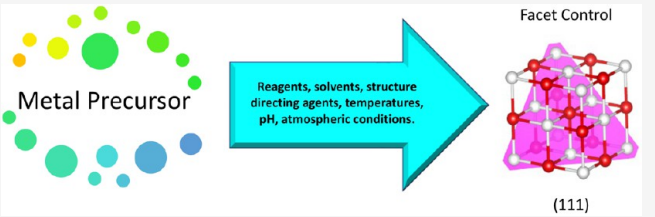




## 1. INTRODUCTION

Metal oxides represent a class of materials with physical and chemical properties that can be altered by manipulation of the morphology and surface structures. Thus, a major active pursuit for chemists is to develop a fundamental understanding of the synthesis/structure property relationships of these materials. As a general class of materials, metal oxides possess a breadth of electronic and physical properties that have enabled their applications in catalysis, adsorption, insulators, semiconductors, glasses, gels, doping agents, etc.[1] Sophisticated design and synthetic strategies toward novel morphologies and compositions of metal oxide nanomaterials are, therefore, critical for continued scientific advancement.

Dependent upon the fundamental property of surface energy, the various facets on a metal oxide may exhibit different or even enhanced physical and chemical properties. Current reviews display both metal and metal oxide nanomaterial design, fabrication, and structure, with an emphasis on a variety of facets (including high-index facets) and catalytic properties, while we have chosen to specifically focus on the (111) facet of metal oxides without bias toward nanosized domains nor catalytic properties/applications.[2−4] (111) Faceted metal oxides have gained attention in recent years owing to new distinguishing properties and performance opposed to their facet counterparts. According to previous reports, exposed surfaces of a crystal are usually stable and chemically less active crystal planes; therefore, it remains a great challenge to develop general methods for the controllable growth of unusual exposed crystal surfaces such as the (111) facet that possesses a high surface energy for many cubic crystal systems and typically has a faster growth rate and is easily lost at the end of material synthesis.[5−8] Thus, the growth rate of these high energy (111) facets must be slowed by specific parameters of a synthetic process such as the selection of structure directing agents, precursors, and reactants, as well as the conditions in which they are mixed in solution (temperature, pH etc.), calcination heating profiles and environments, etc. These synthetic parameters are unique to each faceted material; however, they all generally aid in exposing the (111) facet through reducing the surface energy and stabilizing the facet.

Multiple synthetic methods that yield specific faceted surfaces have been reported; however, the main driving forces(s) and factors that determine their morphology have remained unclear.[8] Because various synthetic methods have proven to be successful in influencing the formation of desired faceted surfaces, this plays a pivotal role in the ability to tailor metal oxides opening a wide avenue for the design of new metal oxides and mixed metal oxides with improved facet-dependent properties for various applications.

Because of the growing scientific interest in metal oxide (111) facets, it is of value to synthetic chemists to consider and venture beyond a materials' most commonly formed facet. However, conceiving and designing synthetic processes for new systems require a deep understanding of the literature and the most influential parameter space. This review aims to alleviate the above issue by providing the reader with a survey of synthetic methods for (111) faceted metal oxides as well as illuminating

**Published:** August 16, 2022

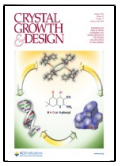







https://doi.org/10.1021/acs.cgd.2c00409
*Cryst. Growth Des.* 2022, 22, 6296−6322

Table 1. Survey of Metal Oxides Discussed with Their Associated Synthetic Methods, Morphology, Structure, and Crystal System

| metal oxide | structure | crystal system | Tasker Type | morphology | synthetic method |
|---|---|---|---|---|---|
| $CeO_2$ (111) | fluorite | cubic | Tasker Type 2 | nanorods | hydrothermal[13] |
| $TiO_2$ (111) | anatase | tetragonal | | nanosheets | hydrothermal[14] |
| $Co_3O_4$ (111) | spinel | cubic | Tasker Type 3 | octahedral nanocrystals | hydrothermal[15] |
| | | | | nanoplates | hydrothermal[16] |
| | | | | octahedral nanoparticles | hydrothermal[17] |
| | | | | atomically thin nanosheets (ATCN) | topochemical conversion[18] |
| MgO (111) | rock salt | cubic | Tasker Type 3 | nanosheets | hydrothermal[19] |
| | | | | nanosheets | hydrothermal aerogel[20] |
| | | | | octahedral particles | thermal decomposition[8] |
| | | | | 2D nanosheets | topochemical conversion[21] |
| | | | | particles | solution combustion[22] |
| NiO (111) | rock salt | cubic | Tasker Type 3 | nanosheets | hydrothermal aerogel[23] |
| | | | | octahedral nanoparticles | water-controlled released solvothermal process (WCRSP) (111)[24] |
| | | | | octahedral particles | thermal decomposition[25] |
| $Fe_3O_4$ (111) | spinel | cubic | Tasker Type 3 | nanoplates, truncated octahedrons, and tetrahedrons | thermal decomposition[26] |
| $LaCoO_3$ (111) | perovskite cobaltite | trigonal | Tasker Type 3 | microcrystalline octahedron | thermal decomposition[6] |
| $La_xSr_{1-x}CoO_3$ (111) | | | | | |
| $Cu_2O$ (111) | cuprite | cubic | Tasker Type 3 | nanospheres | one-pot assembly[27] |
| | | | | microcrystals | one-pot assembly[28] |

the main synthetic factors/parameters that expose these surfaces along with a brief overview of the resulting properties and applications. The synthetic routes discussed herein consist of hydrothermal/solvothermal, thermal decomposition, topochemical conversion, solution combustion, and one-pot assembly methods. The metal oxides discussed cover cubic, trigonal, and tetragonal crystal systems with dominant (111) surface facets.

**1.1. Metal Oxide Structures and (111) Faceting.** The most important and common oxide crystal structures are rock salt, fluorite, spinel, perovskite, wurtzite, rutile, and corundum.[9] The crystal structures discussed here include fluorite, anatase, spinel, rock salt, perovskite cobaltite, and cuprite which crystallize into the cubic crystal system except for anatase and perovskite cobaltite that crystallize into the tetragonal and trigonal crystal system, respectively. Perovskite structures in an ideal fashion crystallize into the cubic system; however, with the addition of more complex ions, the structure distorts.[10] In the case of lanthanum strontium cobaltite (LSCO) or lanthanum cobaltite (LCO), a rhombohedral distorted perovskite structure exists at low temperature, and thus is not cubic but crystallizes into the trigonal crystal system.[11] At higher temperatures such as 900 °C, the rhombohedral distorted perovskite transforms into a cubic perovskite.[12] The metal oxides discussed along with their associated methods, morphology, structure, crystal systems, and Tasker Types can be seen in Table 1.

**1.2. Stable Facets and Implication on Activity.** The thermodynamically stable facet is the one with the lowest surface energy in a given set of conditions. The surface energy is the most important quantity that determines the stability of a given surface orientation which is defined as the work needed to cut a bulk crystal into two equivalent parts, but this becomes complicated with complex metal oxides.[9] In simpler terms, one could imagine the surface energy as the number of bonds needed to be broken per surface area or the number of missing neighbors in the first coordination sphere.[9] The lower the surface energy of the facet, the more thermodynamically stable it is. In the case of binary oxide systems, the number of missing bonds per unit area is not enough to define the surface energy, since deviations from stoichiometry lead to dependence on the chemical potential of one or more of the species (e.g., oxygen), thereby making the thermodynamic stability of a facet dependent on the synthesis conditions.[29] In general, a material grown exposes more than one facet, and usually the facets exposed are not crystallographically equivalent; hence, they have different surface energies. The equilibrium crystal shape is the crystal taken at equilibrium, and that is determined not only by the facet orientation with the lowest energy but several others as well. Such knowledge of the set of available surface energy determines the thermodynamically stable shape via the Wulff construction.[30]

Often the synthesis of nanomaterials is based on understanding and control of kinetic factors during growth, rather than thermodynamic equilibrium. As such, growth rates along different directions become critical factors in determining the facets exposed by a synthesized nanomaterial. For example, a slow growing facet will expand laterally and remain on the final shape. A fast-growing facet will grow along the surface normal too fast and eventually be cut off by the facets that grow laterally. Theoretical understanding of the growth shapes can be obtained from the kinetic Wulff construction assuming the growth rates along different directions are known.[31] The Wulff construction and kinetic Wulff construction can help to determine the eventual crystal shapes; however, they have some drawbacks.[32,33] Research is ongoing, but connections between the surfaces of (111) faceted nanoparticles with energy minimized


https://doi.org/10.1021/acs.cgd.2c00409
Cryst. Growth Des. 2022, 22, 6296−6322

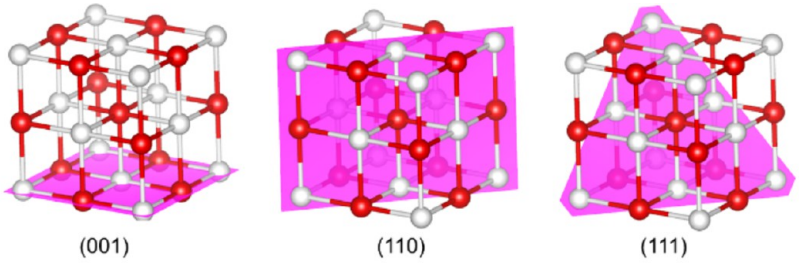


**Figure 1.** Low-index atomic planes for the rock salt structure.

Wulff reconstructions and (111) faceted extended systems (thin films and larger crystals) in which steps, kinks, and extended defects play key roles will likely demonstrate different exposed surfaces.

While providing a fundamental understanding of the growth and facet exposed, the thermodynamic and kinetic Wulff constructions require knowledge of surface energies and growth rates along different directions, respectively. Such quantities are not easy to compute or obtain, especially for oxides and other ceramics. The main reasons for lack of precise knowledge of surface energies and growth rates include variations of stoichiometry, dependence of growth rate on growth condition in each experiment, and concentration of precursors and structure directing agents in solutions. In some cases, surface energies can be obtained using sophisticated search methods, but such knowledge could only be applicable for synthesis methods that aim for near-thermodynamic equilibrium conditions.[34−36] In current practice, researchers employ synthesis methods that allow for ease of control over the composition, shape, and properties of various target nanomaterials. Such methods fall mainly into the category of kinetically controlled methods, for which computations of surface energy in theoretical conditions (zero Kelvin, ideal stoichiometric composition, interface with vacuum, etc.) may not always be useful.

For compounds of the fluorite structure, the most thermodynamically stable facet is the (111) facet.[37−39] It is important to note that enhanced facet-dependent properties, such as catalytic properties, can be potentially related to chemically active sites on high energy facets.[5,16,22] For the case of metal oxides of the fluorite structure, since the most stable facet is the (111) facet, these (111) facets may not exhibit enhanced chemical properties compared to other structures that possess the (100) or (101) facets as their most stable forms. This is seen for example in the carbon monoxide (CO) oxidation activity on ceria. CO oxidation was found to be enhanced and bonded more strongly on ceria reactive rods (110) and ceria cube (100) surfaces than on the less reactive octahedral surface (111).[38]

For the remaining structures described in this review; they contain a facet other than the (111) facet as their most stable facet. For anatase, spinel, rock salt, perovskite cobaltite, and cuprite, the most thermodynamically stable facets under typical conditions are (101), (100), (100), (100), and (100) respectively.[9,26,40−45]

Facet-dependent studies associated with the (111) facet surface on metal oxides have made significant headway in recent years making these materials desirable in not only application but from the perspective of surface scientists and synthetic-structure−property researchers. Anatase $TiO_2$(111) displayed a higher photocatalytic degradation of dyes in aqueous solution compared to that of $TiO_2$(001) and commercial Degussa P25.[14] Spinel $Co_3O_4$(111) nanoplates were found to be more catalytically active toward CO oxidation compared to cobaltite rods with (110) surfaces and cobaltite cubes and spheres with (100) surfaces.[16] Rock salt MgO(111) was found to exhibit a higher catalytic activity for rapeseed oil transesterification compared to its (110) and (100) counterparts.[46] Additionally, adsorptive properties of MgO(111) outperformed nanoscale and bulk MgO both having the (100) facet for carbon dioxide uptake.[47] Even more recently was the study of MgO(111) when exposed to water during 2-pentanone condensation, showing that the (111) facet is more active for ketone condensation than the (100) facet.[48] Perovskite cobaltite (111) materials were shown to have enhanced catalytic activity toward CO oxidation compared to its (100) counterpart.[6] Cuprite (111) materials in both microcrystal and nanosphere morphology have a higher photocatalytic degradation of dyes compared to its (100) counterpart.[27,28]

The above results stress the importance of facet-dependent properties specifically for the (111) facet across various metal oxide structures. The stability of these facets is dependent on the environmental conditions. For example, a recent study has shown that under certain temperatures and pressures the (111) faceted MgO system converts to (100), while in other environments it maintains the faceting and can be reused as a catalyst.[47,49,50]

**1.3. The (111) Facet.** In a cubic system, the (*hkl*) planes are defined by their surface being normal along the [*hkl*] crystallographic direction. The (001), (110), and (111) facets are, respectively, the top face, the plane parallel with the *z*-axis and containing the face diagonal of the base face, and the place containing three face diagonals for the faces that meet that origin. Figure 1 displays the typical low-index atomic planes for the rock salt lattice, which consists of two face-centered cubic lattices (one for anions, one for cations) that are displaced by half of the lattice constant along one of the sides of the conventional cell. These surfaces associated with these low-index planes expose different atomic arrangements, which in turn yield different surface energies and different activities at the surfaces. The orientation of the surface is not sufficient to determine surface energies; the underlying crystal structure is important as well. For example, fluorite (111) and rock salt (111) surfaces are different due to the different bonding in these materials. A potentially helpful way of categorizing the different (111) faceted surface atomic arrangements is by the three different Tasker Types.[51]

Tasker's categorization of surfaces falls into three different types and is widely used to classify the polarity of ionic compound surfaces.[52] In this categorization, the crystal is represented by a stack of planes perpendicular to the surface and are arranged in a way to give an electrostatically neutral building


https://doi.org/10.1021/acs.cgd.2c00409
Cryst. Growth Des. 2022, 22, 6296−6322

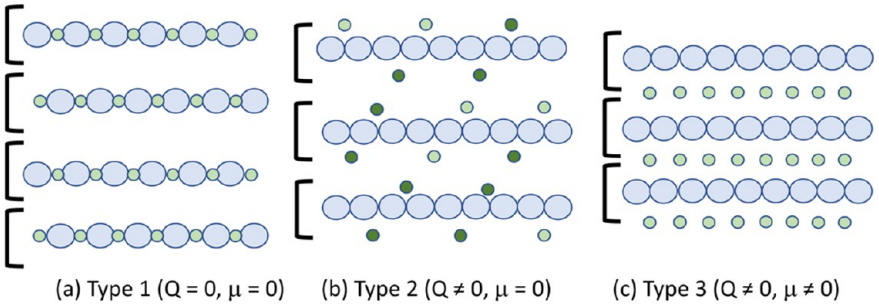


**Figure 2.** (a–c) Classification of oxide surfaces according to Tasker.[51] Here $Q = 0$ indicates no net charge, and $\mu = 0$ indicates no dipole moment perpendicular to the surface. Reprinted (adapted) with permission from ref 9. Copyright 2013 John Wiley and Sons.

block.[9] The planes in a Tasker Type 1 surface have zero charge due to a stoichiometric balance of anions and cations in each plane.[53] In a Tasker Type 2 surface, each plane is charged, but the repeat unit consists of three planes in a symmetric configuration resulting in no net dipole moment perpendicular to the surface.[53] Lastly, a Tasker Type 3 surface consists of alternately charged planes with a repeat unit of only two planes producing a dipole moment perpendicular to the surface.[53] The Tasker types for each metal oxide discussed have been identified in Table 1. However, anatase $TiO_2$ has atomic planes that are not parallel to the (111) surface. This peculiarity of the tetragonal anatase $TiO_2$ leads to inhomogeneities of the charge and dipole along the nominal (111) surface, which make it problematic to classify into the types described in Figure 2. Figure 2 depicts the different oxide surfaces according to the Tasker Type.[9,51]

**1.4. The (111) Facet on Fluorite and Rock Salt Structures.** Stated in a previous review, the rock salt structure is one of the simplest metal oxides having face-centered cubic crystals with one metal ion surrounded by six nearest-neighbor oxygen ions and vice versa.[1] Metal oxides included in this structure are MgO, CaO, NiO, CoO, MnO, SrO, and EuO, which are widely used as catalysts and catalyst supports.[1] Of these rock salt metal oxides described above, MgO is the most studied due to its simplistic structure and high ionic character that makes it a good model compound for computational and surface science studies.[1,20] Early density functional theory studies pioneered the movement toward (111) nanostructuring of rock salt structures via guided synthesis as theoreticians described the (111) surface as a "unique playground for catalysis" and adsorption.[54,55] The (111) facet for rock salt structures is described as a surface containing alternating monolayers of anions and cations creating a strong electrostatic perpendicular to the (111) surface and is a Tasker Type 3 surface.[9,20,46,51] Surface reconstructions of polar facets have received significant attention in the surface science literature and are generally driven by environmental conditions (temperature, pressure, solvent, etc.).[50,56−60] An ideal (111) surface on MgO consists of monolayers of either all anions or cations creating a polar surface.[54] However, these surfaces have been found to be stabilized by hydroxyls suggesting that a bare polar surface facet does not exist, but this is not to discount the enhanced chemical properties that are observed via (111) faceting.[50]

For a fluorite compound, such as $CeO_2$, the various facets of the unit cell structure are shown in Figure 3.[61] The (111) surface of $CeO_2$ is terminated by 3-fold-coordinated oxygen atoms and seven-fold-coordinated cerium atoms, and it is also a nonpolar surface due to a neutral repeated three-plane units cause no net dipole moment thereby resulting in a Tasker Type 2 surface.[51,53,62] Figure 4 depicts $CeO_2$(111) as an unreconstructed Tasker Type 2 surface.[51,53]

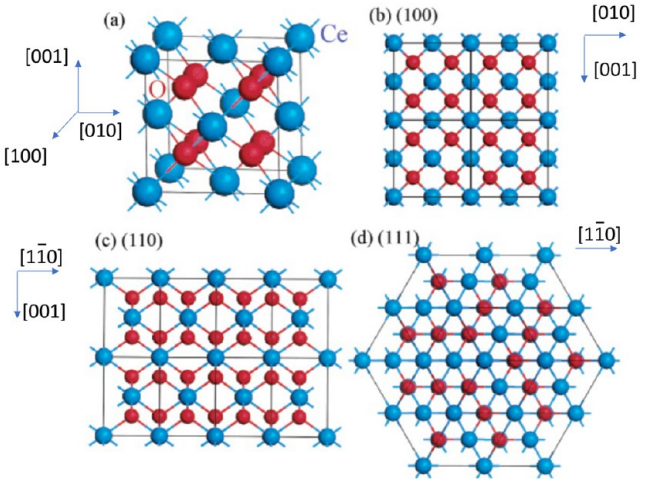


**Figure 3.** (a) Unit cell of the $CeO_2$ structure. (b) The (100) [or (200)], (c) (110), and (d) (111) planes of the $CeO_2$ structure. Reprinted (adapted) with permission from ref 61. Copyright 2003 American Chemical Society.

It can be seen from the above two case studies that the (111) surface on a Tasker Type 3 surface for rock salt and a (111) surface on a Tasker Type 2 surface for fluorite are clearly different in terms of surface atomic arrangements.

## 2. SYNTHETIC METHODS

The synthesis methods described here are categorized into five main types including hydrothermal/solvothermal, thermodecompostion, topochemical conversion, solution combustion, and one-pot assembly methods with most of the case studies falling under hydrothermal/solvothermal methods.

**2.1. Hydrothermal/Solvothermal Method.** Hydrothermal synthesis is known to include various techniques of crystallizing substances from high-temperature aqueous solutions at high pressures. Hydrothermal treatment is regarded as economical and effective as it supports low temperature synthesis and morphological control.[63] In the hydrothermal process, the metal oxide is formed through the dehydration condensation reaction of the hydroxyl groups on the surfaces that form via hydrolysis of the metal salt.[17,64,65]

Solvothermal treatment of materials is very similar to hydrothermal treatment except solvents other than water are utilized. The solvothermal treatment also allows for precise control over the size, shape distribution, and crystallinity of metal oxide nanoparticles or nanostructured materials. These characteristics can be altered by changing certain experimental parameters, including reaction temperature, reaction time, solvent type, surfactant type, precursor type, etc.[66]


https://doi.org/10.1021/acs.cgd.2c00409
Cryst. Growth Des. 2022, 22, 6296−6322

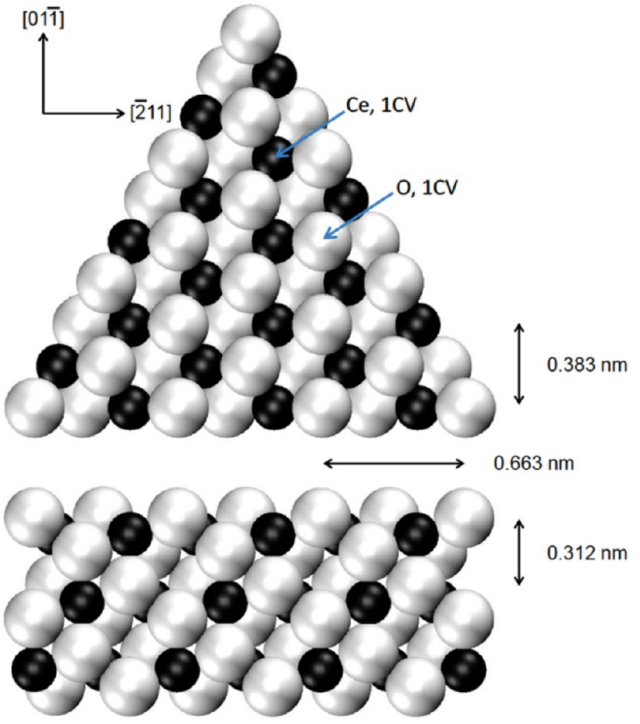


**Figure 4.** $CeO_2$(111) depicted as unreconstructed Tasker Type 2 surface.[51] The black spheres are Ce, and the white spheres are O. The spheres have been drawn at 100% space-filling to indicate accessibility to subsurface sites. CV refers to the number of coordination vacancies around the Ce in the second layer and O in the top layer. Reprinted (adapted) with permission from ref 53. Copyright 2015 Elsevier.

Although the two methods are very similar, it is important to recognize that most scientific accounts do not classify their synthesis strictly according to the above definition, meaning some accounts report on hydrothermal processes yet end up utilizing solvents other than water and thus should actually be termed solvothermal.

*2.1.1. $CeO_2$(111) Nanorods.* Cerium oxide is used in applications such as catalysis, solid oxide fuels, and UV blocking and shielding materials.[63] Mai et al. discovered that hydrothermal treatment yields $CeO_2$ with morphologies of different shapes and sizes including nanopolyhedra, nanorods, and nanocubes by varying the base concentration and temperature.[63]

Adapting Mai et al.'s synthesis, Spezzati and co-workers synthesized $CeO_2$(111) nanorods.[13,63] Cerium nitrate hexahydrate (aq) is added to concentrated sodium hydroxide and stirred for 1 h.[13,63] The mixture is then transferred to a Teflon liner, inserted into a autoclave, and heated to 100 °C for 24 h in an oven under static conditions. The specific temperature of 100 °C was used based on previous studies by Mai et al. as shown in Table 2.[63] After the hydrothermal treatment, the solid products were separated by centrifugation and washed. Lastly, the products were dried at 80 °C in a vacuum oven for 2 h and then calcined at 500 °C for 4 h in a gas flow mixture consisting of helium and oxygen. The ceria nanorods created by this method were then doped with palladium and tested for carbon monoxide (CO) oxidation.[13] Aberration corrected transmission electron microscopy (AC-TEM) images of these samples are shown in Figure 5.

Reasons for (111) facet formation were not elucidated in this case study; however, it can be traced back to Mai et al.'s. synthetic method in that varying the base concentration and temperature during hydrothermal treatment yielded different morphologies.[63] Specifically, a reaction temperature of 100 °C yields ceria rods, whereas a temperature of 180 °C yields cubes. To see this parameter effect, see Table 2 taken from Mai et al.'s synthetic method.[63]

*2.1.2. Anatase $TiO_2$(111) Nanosheets.* Titanium dioxide has long been a great commercial product for use in photocatalysis, cosmetic

**Table 2. Crystal Structures, Shapes, and Sizes of Several $CeO_2$ Samples**[a,b]

| $C_{NaOH}$ (mol $L^{-1}$) | $T$ (°C) | $t$ (h) | shape | size (nm) |
|---|---|---|---|---|
| 0.01 | 100 | 24 | polyhedra | 11.5 ± 1.8 |
| 0.01 | 180 | 24 | polyhedra | 9–25 |
| 1 | 100 | 24 | polyhedral; rods | |
| 3 | 100 | 24 | polyhedral; rods | |
| 6 | 100 | 24 | rods | (9.6 ± 1.2) × (50–200) |
| 6 | 140 | 24 | rods; cubes | |
| 6 | 180 | 24 | cubes | (36.1 ± 7.1) |
| 9 | 100 | 24 | rods | (13.3 ± 2.8) × (100–400) |

[a]Synthesized under $[Ce^{3+}]$ = 0.05 mol $L^{-1}$. [b]Reprinted (adapted) with permission from ref 63. Copyright 2005 American Chemical Society.

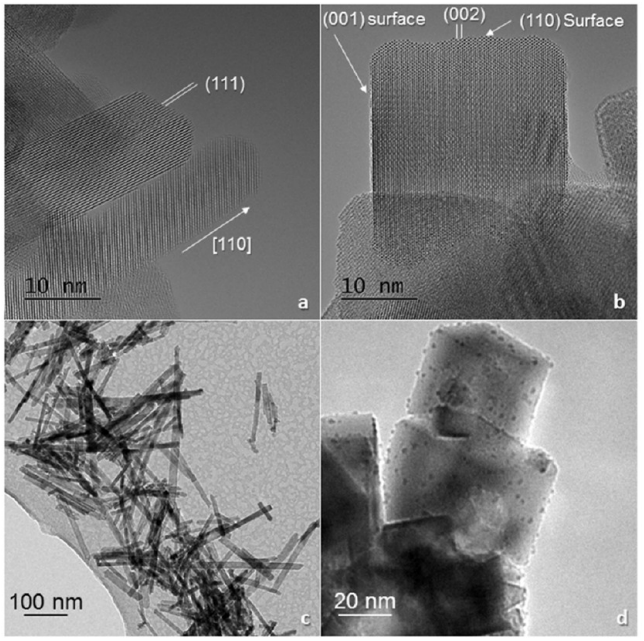


**Figure 5.** AC-TEM images of (a) $CeO_2$-rods and (b) $CeO_2$-cubes with an indication of the most prominent planes, and TEM images of (c) Pd/$CeO_2$-rods and (d) Pd/$CeO_2$-cubes. Reprinted (adapted) with permission from ref 13. Copyright 2019 Elsevier.

products, and other industries. Zhang et al. reported the hydrothermal synthesis of nanoscale anatase $TiO_2$ with dominant (111) facets.[14]

The hydrothermal synthesis is executed by a one-step hydrothermal route utilizing precursors of tetrabutyl titanate ($Ti(OBu)_4$), ammonium fluoride, hydrofluoric acid (40%), and deionized water.[14] Different ratios of $NH_4^+$ and $F^-$ were tested to find the best mole ratio necessary to yield a high percentage of polar surfaces. Tetrabutyl titanate is mixed with ammonium fluoride, hydrofluoric acid, ammonia (28%), and deionized water in a Teflon-lined autoclave and heated to 180 °C for 24 h. The resulting precipitate is then centrifuged, washed in absolute ethanol, and dried at 102 °C for 12 h. The powder is then calcined at 600 °C for 90 min.

Varying the mole ratio resulted in the discovery that polar (111) surfaces can only be obtained when both $NH_4^+$ and $F^-$ are in a 1:2 ratio. Since crystal facets with a low surface energy will predominantly be exposed, this specific mole ratio results in the large percentage of (111) facets being exposed due to surface fluorination, which leads to a reduction of the (111) surface energy. The structural information on the samples prepared at different experimental conditions, different facets of anatase $TiO_2$, surface structure, and HRTEM images of the


https://doi.org/10.1021/acs.cgd.2c00409
Cryst. Growth Des. 2022, 22, 6296–6322

Table 3. Structural Information of the Samples Prepared at Different Experimental Conditions[a]

| sample | phase[b] | relative crystal[c] | $S_{BET}$[d] ($m^3/g$) | (101)[e] (%) | (001)[e] (%) | (111)[e] (%) |
|---|---|---|---|---|---|---|
| T1 | A | 1.26 | 72 | 95 | 5 | |
| T2 | A | 1.18 | 74 | 68 | | 32 |
| T3 | A | 1.07 | 94 | 37 | | 63 |
| T4 | A | 1 | 98 | 30 | | 70 |
| T5 | A | 1.11 | 113 | 24 | 76 | |

[a]Reprinted (adapted) with permission from ref 14. Copyright 2014 Elsevier B.V. [b]A is anatase and R is rutile. [c]This is calculated to compare the intensity of (101) peaks of anatase, and $T_{111-3}$ standard. [d]$S_{BET}$ is the specific surface area. [e]Exposed facets.

product can be seen in Table 3, Figure 6, Figure 7, and Figure 8 respectively.[14]

*2.1.3. $Co_3O_4$(111) Octahedral Nanoparticles.* Cobalt oxide's main applications include, but are not limited to, electrochromics, magnetism, catalysis, chemical industry oxidants, and sensors.[67] A number of synthetic approaches have been reported to realize the $Co_3O_4$(111) octahedral nanoparticles.

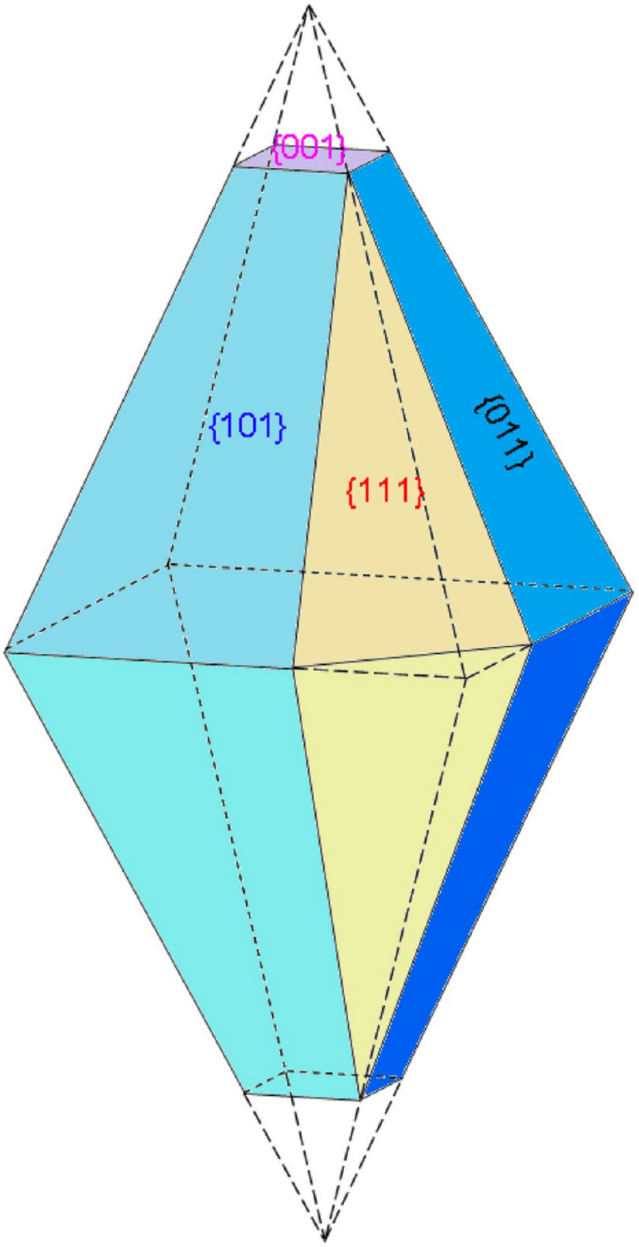


**Figure 6.** Schematic illustration of (101), (011), (001), and (111) facets of anatase $TiO_2$. Reprinted (adapted) with permission from ref 14. Copyright 2014 Elsevier B.V.

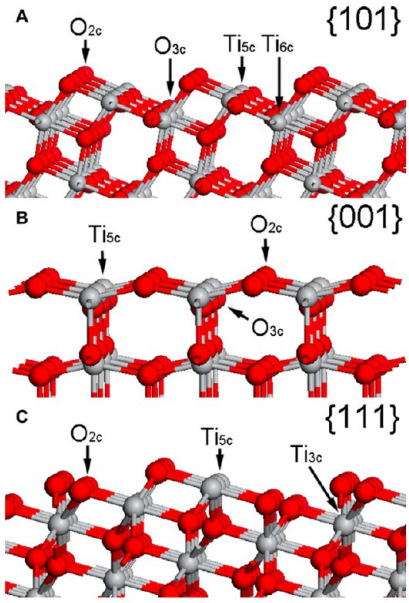


**Figure 7.** Surface structure of (A) (101), (B) (001), and (C) (111) facets on $TiO_2$. Reprinted (adapted) with permission from ref 14. Copyright 2014 Elsevier B.V.

Recently, an intricate and detailed hydrothermal synthesis of euhedral $Co_3O_4$ nanocrystals via nutrient-assisted topotactic transformation under anoxic conditions has been reported.[15] In the above method, cobalt nitrate hexahydrate (nutrient) and sodium hydroxide with a constant ratio of $Co^{2+}$ to $OH^-$ of 2.7 were dissolved in demineralized water.[15] The mixture was then stirred for 5 min and transferred into a 20 mL Teflon lined stainless steel reactor and heated to 180 °C for 0.5, 1, 3, 5, and 8 h at 15 bar to provide the intermediate and final products. For the case of dominant octahedral (111) facets, 3 h at 180 °C is the required time. The precipitate is then separated by centrifugation at 3000 rpm for 5 min and washed with distilled water. The $Co_3O_4$ nanocrystals are then dried at 60 °C overnight.

Keeping the ratio between $Co^{2+}$ to $OH^{-1}$ constant at 2.7, but varying the initial amounts of the starting reagents, resulted in a variety of morphologies indicating that the product morphologies depend on the concentration of the starting precursors rather than their molar ratio. Having a specific starting amount of 4.09 mol $dm^{-1}$ for cobalt nitrate hexahydrate and 1.52 mol $dm^{-1}$ for sodium hydroxide yielded octahedral morphologies with dominant (111) exposed surfaces. The synthesis conditions and yielding morphologies can be seen in Table 4 and Figure 9.

The authors of this study break down the synthesis into detailed steps, and it can be easily visualized in Figure 10 with the three main steps being the formation of the parent reactive template (PRT), nutrient-mediated topotactic nucleation (NTN), and morphogenesis on nanocrystals (MNC) in that specific order. The main factors yielding dominant (111) exposed surfaces with an octahedral shape appear to be


https://doi.org/10.1021/acs.cgd.2c00409
Cryst. Growth Des. 2022, 22, 6296−6322

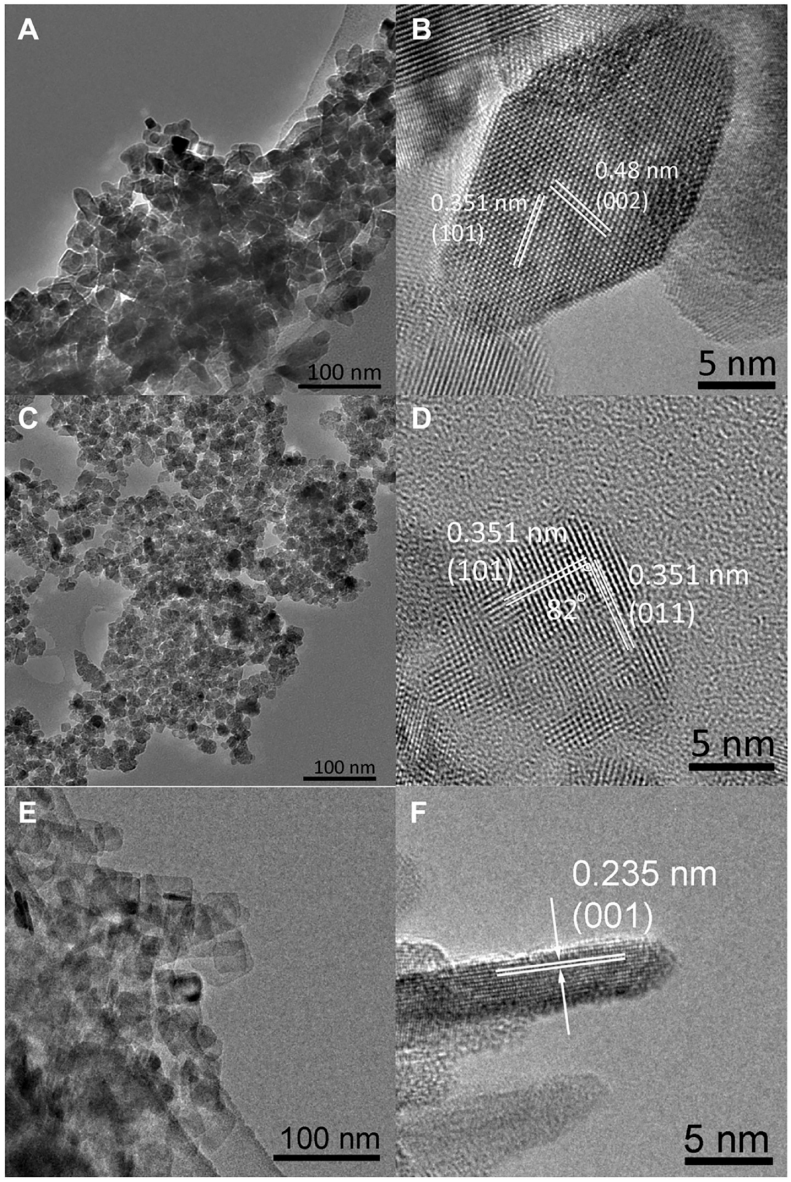


**Figure 8.** HRTEM images of T1 (A) low resolution, (B) high resolution; T4 (C) low resolution, (D) high resolution, and T5 (E) low resolution, (F) high resolution. Reprinted (adapted) with permission from ref 14. Copyright 2014 Elsevier B.V.

**Table 4. Synthesis Conditions Leading to Cubic, Cuboctahedral, and Octahedral Shapes of Cobalt Spinel Nanocrystals**[a,b]

| morphology | $c_{Co^{2+}}$ (mol $L^{-1}$) | $c_{OH^-}$ (mol $L^{-1}$) | $c_{Co^{2+}}/c_{OH^-}$ | $\Delta c_{Co^{2+}}$ |
|---|---|---|---|---|
| cubic | 1.31 | 0.49 | 2.7 | 1.07 |
| cuboctahedral | 2.69 | 1.00 | 2.7 | 2.19 |
| octahedral | 4.09 | 1.52 | 2.7 | 3.33 |

[a] $c_{Co^{2+}}$ and $c_{OH^-}$ indicate the initial concentration of cobalt nitrate and sodium hydroxide, respectively, whereas $\Delta c_{Co^{2+}}$ stands for change in the $Co^{2+}$ aq concentration in the mother liquor after precipitation of the parent cobalt hydroxide. [b] Reprinted (adapted) with permission from ref 15. Copyright 2020 American Chemical Society.

the constant ratio of $Co^{2+}$ to $OH^-$ of 2.7 and the high concentration of nutrient ($NO_3^-$ anions) playing a key role as an oxidant, an oxygen donor, and by influencing the surface energy evident of a structure/shape directing agent.[15]

In another study, Zhou et al. reported the synthesis of octahedral $Co_3O_4$ enclosed by (111) facets via a one-step hydrothermal method.[17] The (100) facet on $Co_3O_4$ leads to a cubic structure while the (111) facet leads to an octahedral structure. The (111) facet formation on $Co_3O_4$ is faster growing than that of the (100) facet; therefore, slowing down this competitive growth can yield a different structure with an unconventional facet (i.e., octahedral structure enclosed by (111) facets).[17]

To synthesize octahedral $Co_3O_4$ nanoparticles with (111) facets, 0.4 mM triphenylphosphine ($PPh_3$) and 1.7 mM cobalt(II) nitrate hexahydrate were first dissolved in 120 mL of ultrapure water under ultrasonic conditions. The pH value was then adjusted to 7.6 by the addition of an aqueous solution of 2 M sodium hydroxide. The solution was then transferred to a 150 mL Teflon-lined autoclave and heated to 180 °C for 24 h. The autoclave was allowed to cool to room temperature, and the products were then centrifuged and washed with ultrapure water and absolute ethanol and finally dried in air at 80 °C for 6 h.

It was found that by varying reaction parameters such as the pH, molar ratio of $PPh_3$, the reaction temperature, and time greatly affected


https://doi.org/10.1021/acs.cgd.2c00409
Cryst. Growth Des. 2022, 22, 6296−6322

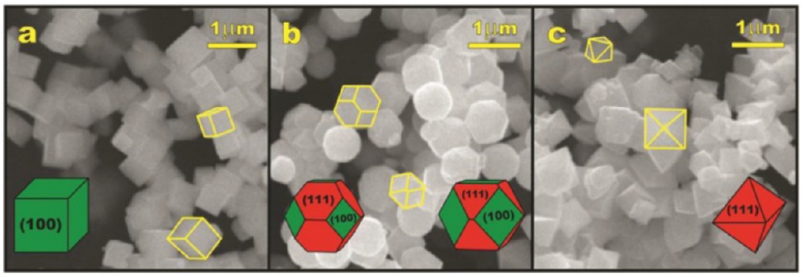


**Figure 9.** Polyhedral morphology of the cobalt spinel nanocrystals obtained under different hydrothermal synthesis conditions, (a) cubic shape obtained at $c_{Co^{2+}} = 1.21$ mol $L^{-1}$; (b) cuboctahedral at $c_{Co^{2+}} = 2.69$ mol $L^{-1}$; (c) octahedral shape at $c_{Co^{2+}} = 4.09$ mol $L^{-1}$. In all syntheses, a constant $c_{Co^{2+}}/c_{OH^-}$ ratio equal to 2.7 was maintained. Reprinted (adapted) with permission from ref 15. Copyright 2020 American Chemical Society.

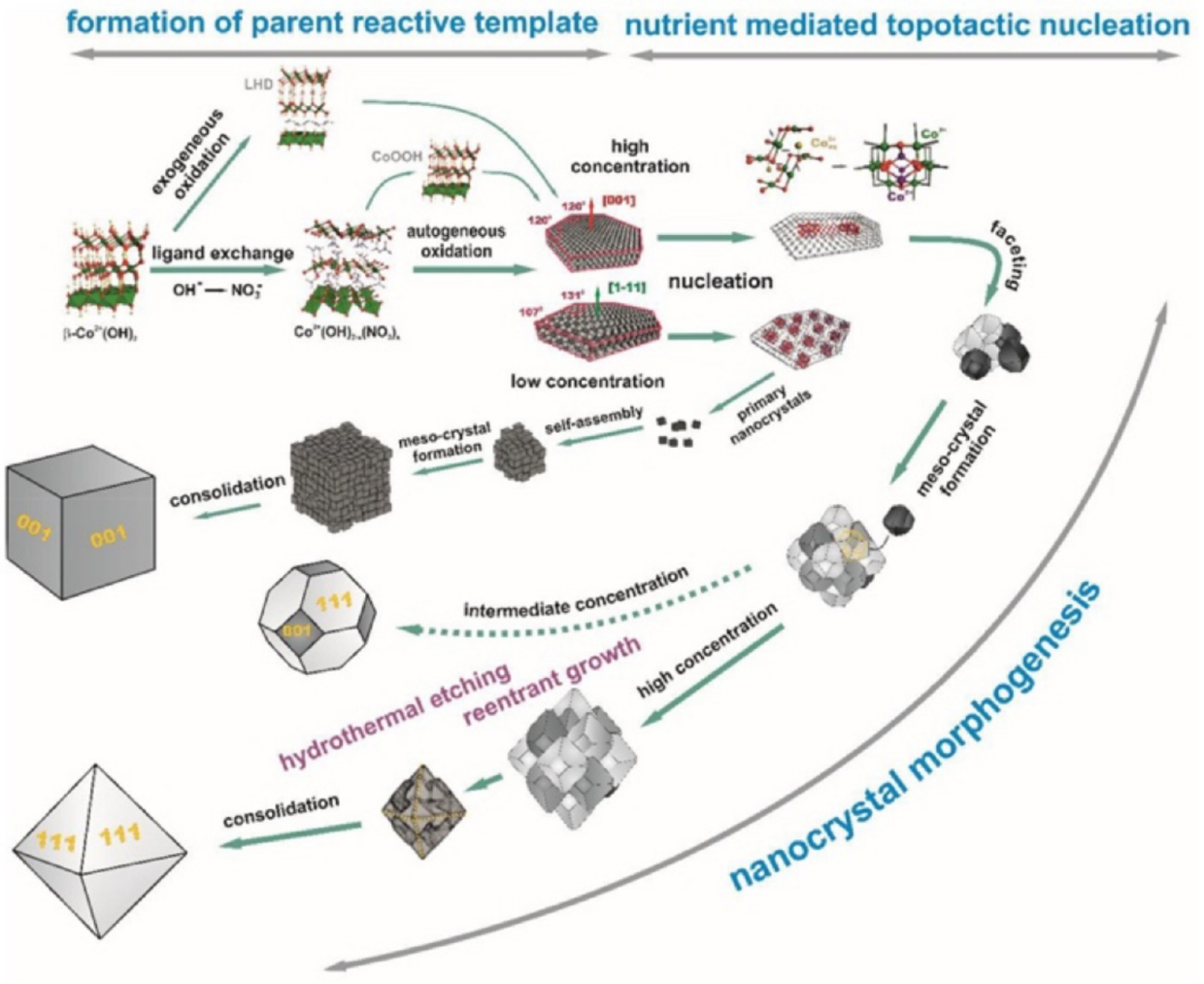


**Figure 10.** A series of structural and morphological changes leading to the development of cobalt spinel sub-micrometer crystals from the precipitated $\beta$-$Co(OH)_2$ under hydrothermal conditions. The principal stages of the reaction include the formation of the parent reactive template (top left), nutrient-assisted topotactic nucleation (top right), and nanocrystal morphogenesis (bottom), leading to the development of cubic (low concentration of nutrient), truncated octahedral (medium concentration), and octahedral shapes of $Co_3O_4$ (high concentration). At the top of the NTN section, the displacement of the cobalt cations during the topotactic transformation (in the directions indicated by green arrows), which gives rise to the formation of a core atomic arrangement of the spinel framework, is shown. Reprinted (adapted) with permission from ref 15. Copyright 2020 American Chemical Society.

the product. Since the (111) facet of $Co_3O_4$ is oxygen terminated (see Figure 11), the $O^{2-}$ anion exists in the form of hydroxyl groups in aqueous solution, and thus, the pH can strongly affect the state of the hydroxyl groups and the final product. When the pH is maintained at exactly 7.6, it provides the system with the appropriate amount of $OH^-$ ions, which contributes to the formation of the growth unit, $[Co(OH)_x]^{h-x}$, the adsorption of the growth unit in the form of $[Co(OH)_a(H_2O)_b(PPh_3)_{x-a-b}]^{h-a}$ ($h = 2$ or 3; $x = 4$ or 6; $0 \le a, b \le x$), and the formation of the $Co_3O_4(111)$ octahedra.[17]

The molar ratio of $PPh_3$, like the pH, was also found to have a crucial role in exposing the (111) facet. More than 80% of octahedral nanoparticles could only be formed when the molar ratio of $PPh_3$ to $Co^{2+}$ was kept at 0.26. It was hypothesized that, when $PPh_3$ was in excess, the concentration of growth units, [Co-


https://doi.org/10.1021/acs.cgd.2c00409
Cryst. Growth Des. 2022, 22, 6296−6322

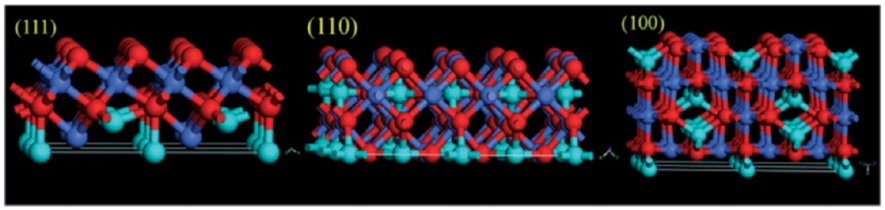


**Figure 11.** Atomic structures of (111), (110), and (100) facets of $Co_3O_4$. The red, blue, and cyan balls represent O, $Co^{3+}$, and $Co^{2+}$, respectively. Reprinted (adapted) with permission from ref 17. Copyright 2013 Royal Society of Chemistry.

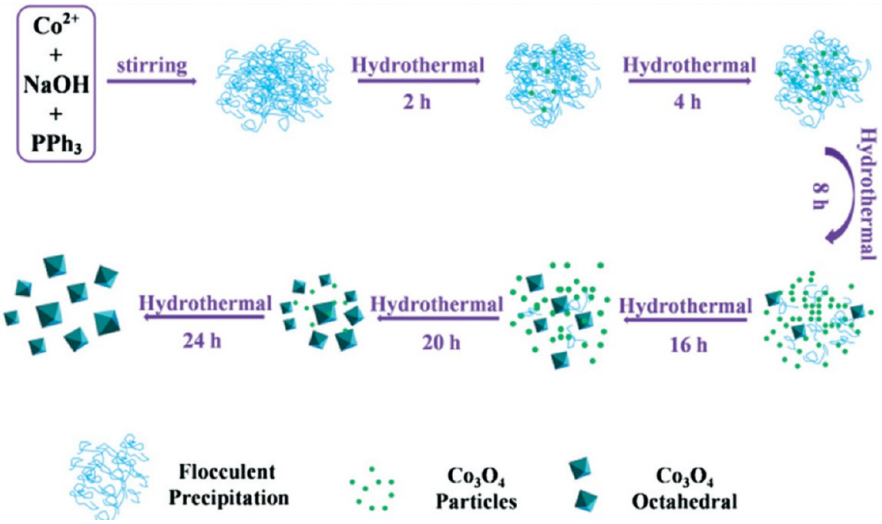


**Figure 12.** Formation process of the as-prepared octahedral $Co_3O_4$ nanoparticles. Reprinted (adapted) with permission from ref 17. Copyright 2013 Royal Society of Chemistry.

$(OH)_a(H_2O)_b(PPh_3)_{x-a-b}]^{h-a}$, would be way too high and would adsorb on other planes besides the (111) facet in which cubes would appear. When the $PPh_3$ was limited, the growth units were also limited in that they could not cover the majority of the (111) facets leading to irregular polyhedra. As stated previously, the (111) facet possesses a maximum density of surface hydroxyl groups. This allows growth units of $[Co(OH)_a(H_2O)_b(PPh_3)_{x-a-b}]^{h-a}$ to be absorbed on the hydroxyl groups and replaces them, thus retarding the growth of the (111) facets. The interaction of $PPh_3$ with surface hydroxyl groups in the appropriate molar ratio is therefore critical for (111) facet exposure.[17]

The reaction temperature and time on the other hand are the most straightforward and simplistic synthetic parameters. Octahedral enclosed facets were formed due to $PPh_3$ being insoluble in water at room temperature and having a flash point of 180 °C. At 180 °C, the dissolved $PPh_3$ can supply the appropriate amount of $[Co(OH)_a(H_2O)_b(PPh_3)_{x-a-b}]^{h-a}$ necessary for octahedral formation. At higher temperatures, irregular polyhedra are formed, and at lower temperatures, cubes are formed. In terms of reaction time, longer amounts of time are needed to convert the metal-hydroxide to its oxide form, and 24 h was deemed suitable.[17]

The pH and molar ratio of triphenylphosphine were the most complex parameters in this study dictating the (111) facet exposure and provide insight into how certain synthetic parameters are indeed crucial for exposing unconventional facets. The formation process depicted in Figure 12 is broken down into three parts: flocculent formation due to sodium hydroxide addition, polycondensation reaction and dissolution of cobalt(II) hydroxide under hydrothermal treatment, and adsorption of growth units containing $PPh_3$ on the (111) facets of $Co_3O_4$, which aided in slowing down the growth of the (111) facets.[17]

*2.1.4. $Co_3O_4$(111) Nanoplates.* Specifically, plate-like nanocrystalline $Co_3O_4$ materials with dominant (111) exposed planes were synthesized in aqueous solution via a hydrothermal process.[16] The amounts of cobalt(II) chloride hexahydrate and polyvinylpyrrolidone (PVP) are dissolved in distilled water to a form a red solution (solution 1). Solution 2 consists of potassium hydroxide dissolved in distilled water and is added to solution 1 and stirred for 30 min. The suspension is then aged at 293 K for 12 h in a Teflon-lined autoclave. The product is then centrifuged and washed with distilled water followed by ethanol and dried at 333 K for 12 h and calcined in air at 573 K for 2 h at a ramp rate of 373 K/h to produce $Co_3O_4$(111) nanoplates. Images of the products can be seen in Figure 13. Among the various nanocrystals Teng et al. synthesized, the $Co_3O_4$(111) nanoplates displayed the highest catalytic activity for CO oxidation, and this was hypothesized to be due to the retainment of (111) active surfaces when dry reactant gases streams are utilized.[16]

*2.1.5. MgO(111) Nanosheets via Ligand Exchange and Esterification.* MgO has been synthesized hydrothermally with its (111) surface exhibiting novel properties that have led to its use in a range of new applications including carbon capture, battery electrolytes, electrochromics, and catalysis.[47] In this case study, Zhu et al. synthesized MgO(111) nanosheets from a direct bottom-up synthesis via ligand exchange and esterification using magnesium acetate tetrahydrate as a precursor under solvothermal conditions and benzyl alcohol as a structure directing agent.[19]

The MgO(111) nanosheets are synthesized by stirring a methanol solution of magnesium acetate tetrahydrate and benzyl alcohol for 5 h. The amount of benzyl alcohol added is the same molar amount with respect to magnesium added. The solution is then transferred to a Teflon-lined steel autoclave and heated in an oven at 180 °C for 48 h. The maximum pressure of the autoclave used was 100 bar, and the filling degree was kept below 60%. The powder is then collected by filtration and washing with methanol and dried at 60 °C for 24 h. The powder is then calcined in a muffle oven at 550 °C for 4 h with a ramp rate of 3 °C/min.

Reasons for (111) facet formation include the fact that a ligand exchange between $CH_3COO^-$ and $CH_3O^-$ is able to take place at the same time that an esterification of $CH_3COO^-$ to $CH_3CO_2CH_3$ takes place, yielding the metastable $Mg(OH)(OCH_3)$ intermediate that will


https://doi.org/10.1021/acs.cgd.2c00409
Cryst. Growth Des. 2022, 22, 6296−6322

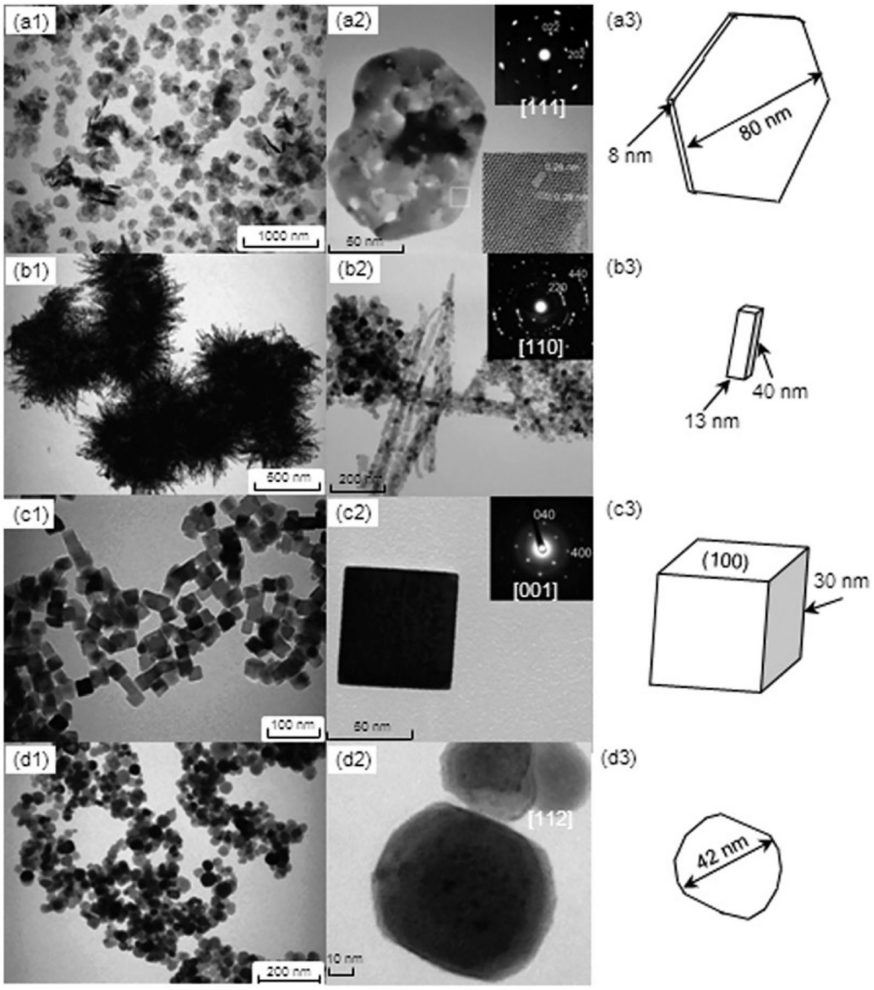


**Figure 13.** TEM images, selected-area electron diffraction (SAED) patterns, and illustrations for $Co_3O_4$ NCs with different shapes: (a1−a3) plate; (b1−b3) rod; (c1−c3) cube; (d1−d3) sphere. Image reprinted (adapted) with permission from ref 16. Copyright 2011 Royal Society of Chemistry.

decompose into MgO and retain (111) nanosheets.[19] It is also important to note that when the $Mg(OH)(OCH_3)$ intermediate is formed, $H_2O$ is a byproduct, and it had previously been speculated by the same author to have a crucial role in the formation of the (111) facet.[20]

It is of relevance to state that this method compared to the one described below is advantageous in that an inert atmosphere is not needed; however, it does result in a lower surface area. In this case study, vanadium oxide supported on MgO(111) superseded that of conventional MgO in the (100) facet for the oxidative dehydrogenation of ethylbenzene with carbon dioxide.[19]

*2.1.6. MgO(111) Nanosheets.* The same authors, Zhu et al., reported the hydrothermal aerogel synthesis of MgO(111) as follows: magnesium ribbon is cut into small pieces and dissolved in absolute methanol under argon and stirring.[20] A templating structure directing agent, 4-methoxybenzyl alcohol, is then added to the mixture in a magnesium:4-methoxybenzyl alcohol ratio of 2:1. After 5 h, a solution of deionized water (molar ratio of 2:1 with respect to magnesium) in methanol is added dropwise. The mixture is then stirred for 12 h and then transferred to an autoclave. The mixture is purged with argon for 10 min and pressurized to 10 bar before heating to 265 °C for 15 h. After 15 h, the vapor is subjected to ventilation in a process known as supercritical fluid drying. The powder is collected and calcined at 500 °C for 6 h. The (111) facet of MgO and HRTEM images can be seen in Figures 14 and 15.

Zhu et al. hypothesized that water plays an important role in the formation of the (111) polar surface because a C−C bond formation can prevail in the water-free system instead of an acid−base interaction

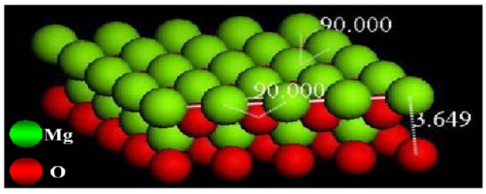


**Figure 14.** Illustration of the (111) facet of MgO (note the alternating layers of $Mg^{2+}$ and $O^{2-}$ ions). Reprinted (adapted) with permission from ref 20. Copyright 2006 John Wiley and Sons.

between the solid powder and benzyl alcohol.[20] Comparison of their work among others suggests that the acid−base interaction between the intermediate, $Mg(OH)(OCH_3)$, and benzyl alcohol is essential for the formation of MgO nanosheets in the (111) facet.[19,20] Until present, the exact role the structure directing agent and water has on the formation of the (111) facet has remained unknown and an active research pursuit, but it has been implied among various reports that residual water in the reaction system may be beneficial for (111) facet exposure on rock salt structures.[8,20,50,55]

*2.1.7. NiO(111) Nanosheets.* Like MgO(111) above, NiO(111) can also be formed via a hydrothermal aerogel synthesis. NiO possesses unique chemical and magnetic properties with applications in a variety of fields such as catalysis, electrochromic, fuel cell electrodes, etc.[23] Further, MgO and NiO have nearly identical lattice parameters but very different electronic properties (MgO large bandgap insulator and NiO


https://doi.org/10.1021/acs.cgd.2c00409
Cryst. Growth Des. 2022, 22, 6296−6322

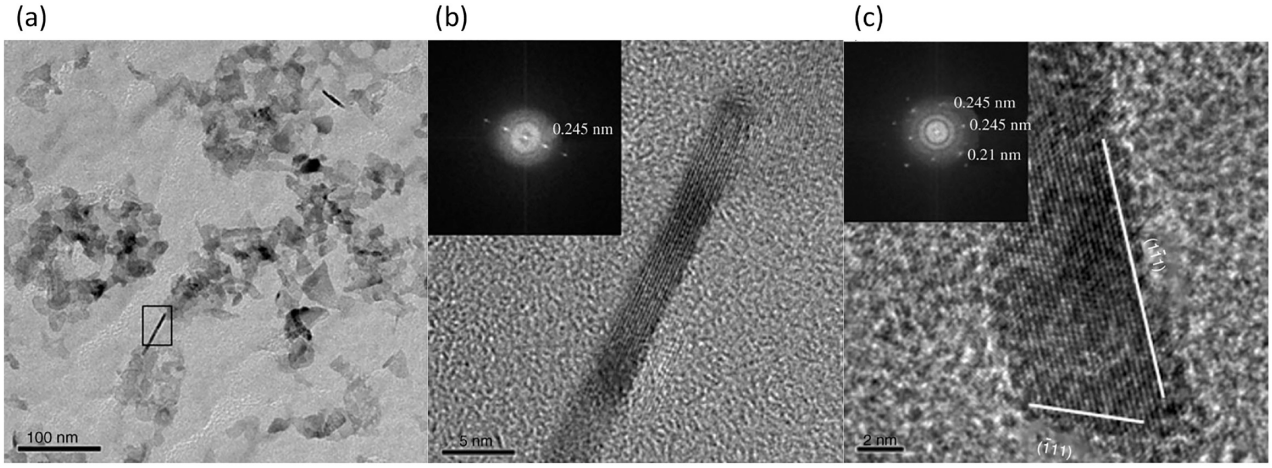


**Figure 15.** (a) BF-TEM images showing larger aggregates and scattered small aggregates of MgO(111) from 4-methoxylbenzyl alcohol. (b, c) HRTEM images and local Fourier transforms of two isolated MgO nanosheets corresponding to the marked area in (a). Reprinted (adapted) with permission from ref 20. Copyright 2006 John Wiley and Sons.

semiconductor with d orbitals). Thus, these two systems allow probing of geometric vs electronic effects.

Hu et al. reported for the first time the synthesis of NiO(111) nanosheets with hexagonal holes.[23] In this method, nickel nitrate hexahydrate is dissolved in absolute methanol. Once dissolved, urea and the structure directing agent, benzyl alcohol, is added to the mixture in a molar ratio of Ni:urea:benzyl alcohol = 1:0.5:2. The mixture is stirred for 1 h and then transferred to an autoclave where it is purged with 7500 Torr of Ar five times and pressurized. The mixture is then heated to 200 °C for 5 h and then to 265 °C for 1.5 h, followed by venting of the pseudo-supercritical vapor. The powder is then collected and calcined in air at a ramp rate of 3 °C/min to 500 °C and held for 6 h.

The parameters crucial for the formation of the (111) facet was determined to be the use of benzyl alcohol as the structure directing agent as well as urea. When benzyl alcohol was not used, no NiO nanosheets with hexagonal holes were formed. In the absence of urea, the nanosheets with hexagonal holes were found to be much larger in the micrometer size range. Therefore, the use of benzyl alcohol assisted in forming the exposed (111) nanosheets with hexagonal holes, and the increase in urea concentration aided in decreasing the size of the nanosheets down to the nanodomain.[23] The HRTEM images, XRD pattern, and space-filling structural model of this product can be seen in Figure 16.

*2.1.8. NiO(111) Octahedral Nanoparticles.* Hermawan et al. synthesized NiO(111) from the transformation of NiOHCl created by a water-controlled release solvothermal process (WCRSP).[24] Water is involved in this process due to the esterification reaction between alcohols and carboxylic acids to release a gradual amount of water molecules to hydrolyze metal precursors such as alkoxides, chlorides, carboxylates, etc.[68−71]

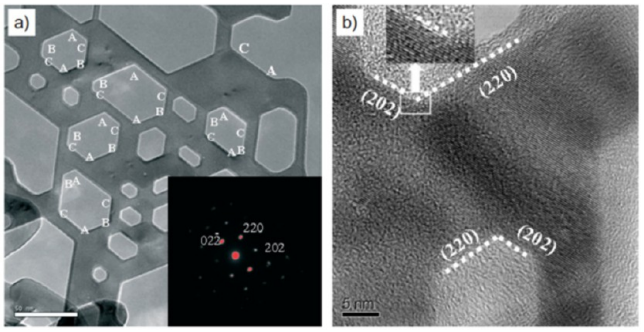


**Figure 16.** (a) TEM image and ED pattern of an individual NiO nanosheet. (b) HRTEM image of a NiO nanosheet; the inset shows the marked edge of a hexagonal hole. Reprinted (adapted) with permission from ref 23. Copyright 2008 John Wiley and Sons.

To start, anhydrous nickel(II) chloride is dissolved in 1-propanol anhydrous under stirring at a speed of 500 rpm for 25 min at room temperature. Next, anhydrous acetic acid is added under the same stirring and speed conditions. The solution is then transferred to a 100 mL Teflon-lined autoclave and solvothermally treated at 200 °C for 10 h and afterward allowed to cool to room temperature. The powder is collected via vacuum-filtration, dried at 60 °C, and ground using a mortar. This whole process yields the precursor, NiOHCl, which is then calcined at 400 °C for 3 h to obtain octahedral nanoparticles of NiO with exposed (111) facets. Images of the product and synthetic scheme can be found in Figure 17.

It was found that the NiO(111) facet could only be formed by NiOHCl and not by b-Ni$(OH)_2$ even though both precursors possess similar layer structures. The precursors differ only by anions $Cl^-$ and $OH^-$ respectively. Hermawan et al. speculated that the reason for (111) facet formation could be due to the possibility of $Cl^-$ acting as a capping agent for $Ni^{2+}$ during the calcination process since the Ni atom is abundant in a clean (111) surface.[24] It is possible that the $Cl^-$ attached to and coordinated with Ni by electronic interaction and inhibited the growth of NiO in the (111) direction thereby lowering the surface energy.[24]

**2.2. Thermal Decomposition Method.** Thermal decomposition is a chemical decomposition caused by heat in either aqueous or nonaqueous solutions. This method utilizes high heating furnaces and can be tuned by varying the atmosphere or flow of gas through the system to yield materials with defined morphologies and structures; however, other heating apparatuses can be used such as hot plates, heated reflux systems, etc. Thermal decomposition by the molten salt route is considered a nonaqueous method to prepare inorganic materials. The salts, hydroxides, deep eutectic mixtures, and ionic liquids used during this method can all potentially be recycled. Previous studies report the colloidal stability of dispersed metal oxide particles in these types of media can allow for the recrystallization of nanoparticles to expose desired facets.[8,72−75]

*2.2.1. $Fe_3O_4$(111) Nanoplates, Truncated Octahedrons, and Tetrahedrons.* Iron oxide has applications in magnetic storage, biosensing, catalysis, and biomedical applications due to its abundance and relative lack of toxicity.[76−81] Until recently, it has been a challenge to control the shape of metal oxides due to metal−oxygen covalent bonding and a diverse crystal packing structure.[7,82] Specifically for iron oxide, controlling the shape of the material on the nanoscale is problematic due to spin-exchange coupling and magnetocrystalline anisotropy effects; however, a thermal decomposition based synthetic method has circumvented this issue.[83]


https://doi.org/10.1021/acs.cgd.2c00409
Cryst. Growth Des. 2022, 22, 6296−6322

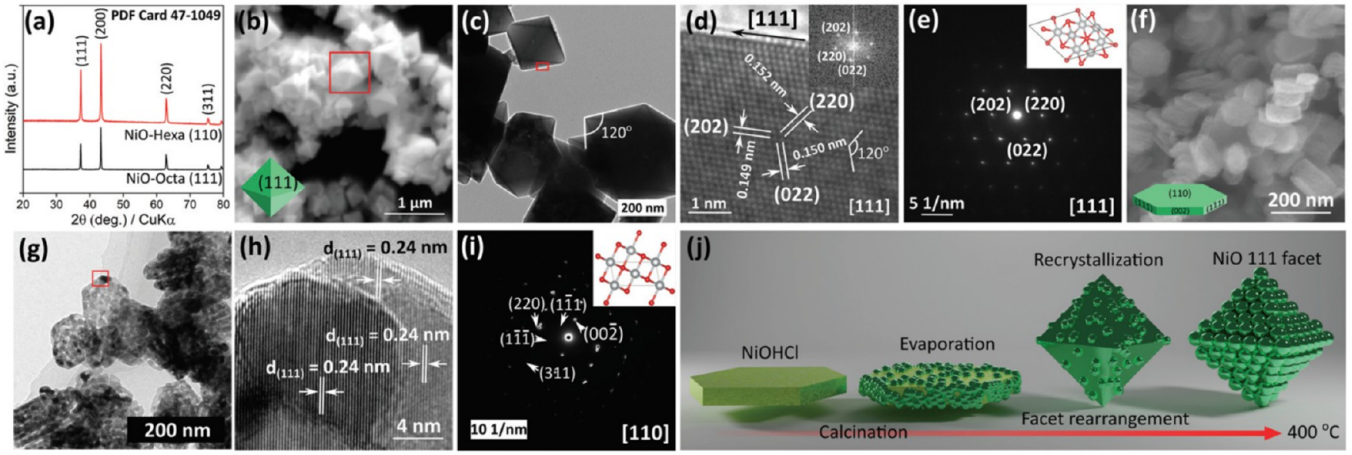


**Figure 17.** (a) XRD patterns of NiO octahedral (111) and NiO hexagonal (110). (b) SEM image, (c) TEM image, (d) HRTEM image (inset is FFT), and (e) SAED pattern taken from the red area (inset is corresponding crystal structure with cutoff in the [111] zone axis) of the NiO-Octa (111) sample. (f) SEM image, (g) TEM image, (h) HRTEM image, and (i) SAED pattern taken from the red area (inset is corresponding crystal structure with cutoff in the [110] zone axis) of the NiO-Hexa (110) sample. (j) Simplified illustration of morphological transformation of the NiOHCl hexagonal morphology into the NiO octahedral morphology. Reprinted (adapted) with permission from ref 24. Copyright 2020 Royal Society of Chemistry.

Zhou et al. reported the thermal decomposition of iron oleate (FeOL) in the presence of sodium oleate (NaOL) yielded $Fe_3O_4$ (IO) plates, truncated octahedra, and tetrahedra all possessing the (111) facet.[26] In their method, iron oleate is first created through reflux and serves as a precursor.

$Fe_3O_4$ nanoplates are made by adding the FeOL precursor and 30 mg (0.1 mmol) of NaOL into a flask containing 15 mL of 1-octadecane (ODE) and in the presence of 159 $\mu$L (0.5 mmol) of oleic acid as a surfactant. Under a nitrogen atmosphere, the flask is heated to 300 °C with a heating rate of 5 °C/min and held for 2 h and refluxed for an additional 30 min before returning to room temperature. The products are precipitated by adding isopropanol and redispersed in hexane.

To yield $Fe_3O_4$ truncated octahedra, a similar method as the plates above was utilized except now 60 mg (0.2 mmol) of NaOL is used. The flask is filled with nitrogen atmosphere and heated to 300 °C with a heating rate of 5 °C/min and held for 2 h and refluxed for an additional 30 min before cooling down to room temperature. Products are precipitated using the same procedure above.

Lastly, $Fe_3O_4$ tetrahedra with preferentially exposed (111) facets were achieved by meticulous control of the conditions to eliminate or minimize heterogeneous growth on different facets. Like the nanoplates synthesis, 180 mg (0.6 mmol) of NaOL is added to the flask containing 900 mg (1 mmol) of FeOL, 159 $\mu$L (0.5 mmol) of oleic acid, and 15 mL of ODE. A nitrogen atmosphere is created, and the flask is heated to 300 °C with a heating rate of 5 °C/min and held for 6 h and refluxed for an additional 30 min and cooled down to room temperature and precipitated using the same procedure as for the nanoplates.

The formation of the $Fe_3O_4$(111) facet exposed products, HRTEM images, and reaction conditions can be found in Figures 18 and 19, and Table 5 respectively. The metal packing density in the *fcc* system is 0.114, 0.102, and 0.053 $Å^{-2}$ for low index facets (111), (100), and (110) respectively. The attachment energy on the $Fe_3O_4$(111) plane is $-11.85$ J/m$^2$ and is the lowest compared to the (100) and (111) planes with attachment energies of ($-3.78$ J/m$^2$) and ($-4.77$ J/m$^2$) respectively.[26,84] It was found that with an increase in the molar ratio between NaOL:FeOL, more predominant (111) exposed surface facets were formed having ratios of (1:10), (2:10), and (6:10) for plates, truncated octahedrons, and tetrahedrons respectively. This trend was linked to the ability of NaOL to regulate the surface energy required to form the $Fe_3O_4$(111) facet. Zhou et al. speculated that this is most likely due to the selective binding of free ionic $OL^-$ to iron ions on the plane and linked to the facets highest iron ion density and lowest attachment energy.[26] Free $OL^-$ are most likely present due to adding NaOL, since it was previously found that NaOL is prone to being ionized and

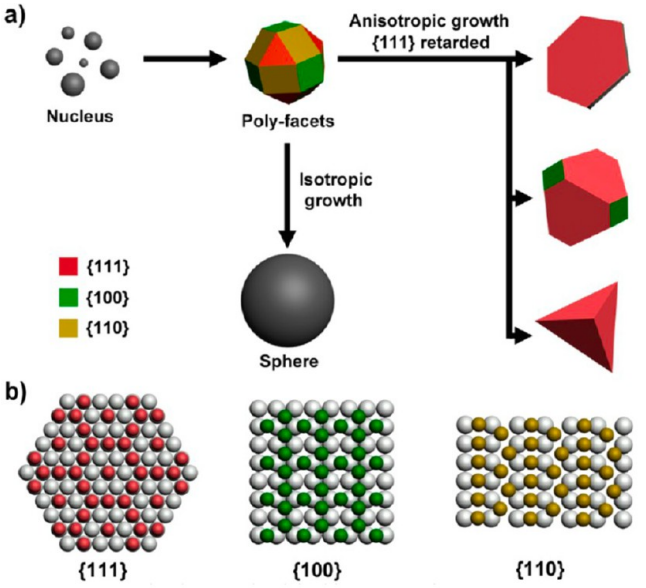


**Figure 18.** Illustration of the formation of $Fe_3O_4$(111) facet exposed IO plates, truncated octahedrons, and tetrahedrons in ODE solvent (a relatively mild condition). (a) Poly facets are basic units from the nucleus, which form spherical IO NPs undergoing an isotropic growth process in the presence of OA as only surfactant. When added with NaOL in the reaction, anisotropic growth happens and leads to formation of IO plates, truncated octahedrons, and tetrahedrons with an increase in the amount of NaOL. (b) Models show a metal package on the outermost layers of the $Fe_3O_4$(111), $Fe_3O_4$(100), and $Fe_3O_4$(110) facets. The white spheres represent oxygen atoms, and colored spheres represent iron atoms in different facets. Reprinted (adapted) with permission from ref 26. Copyright 2015 American Chemical Society.

dissociated into $Na^+$ and $OL^-$ at high temperature implying that remaining unreactive NaOL has the capability to impact the synthesis.[26,43]

*2.2.2. MgO(111) Particles.* Susman et al. conducted extensive studies on the thermal decomposition of different MgO precursors via the molten salt route utilizing molten nitrates (lithium nitrate or combination of sodium nitrate and potassium nitrate) and molten


https://doi.org/10.1021/acs.cgd.2c00409
Cryst. Growth Des. 2022, 22, 6296−6322

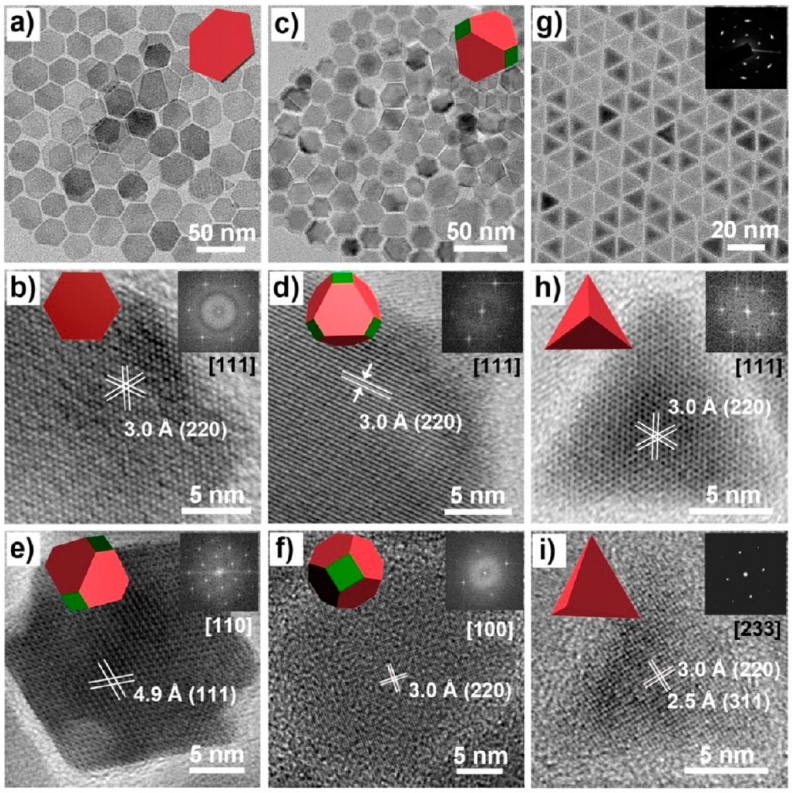


**Figure 19.** TEM and HRTEM images of (a, b) IO plates, (c–f) truncated octahedrons, and (g–i) tetrahedrons obtained in ODE solvent. The side lengths of IO plates, truncated octahedrons, and tetrahedrons are about 20, 16, and 15 nm, respectively. Interplanar distances of 3.0, 4.9, and 2.5 Å are assigned to (220), (111), and (311) planes of $Fe_3O_4$ (magnetite) crystal, respectively. The SAED pattern of IO tetrahedrons (g, inset) indicates a preferential (111) orientation. Insets show FFT patterns along different zone axes and the carton models corresponding to the HRTEM images (b, d–f, h, i). Green and orange colors in carton models represent $Fe_3O_4$(100) and $Fe_3O_4$(111) facets, respectively. Reprinted (adapted) with permission from ref 26. Copyright 2015 American Chemical Society.

**Table 5. Summary of Reaction Conditions for the Synthesis of Various Shaped IO Nanostructures**[d]

| Solvent[a)] | FeOL (mg) | NaOL (mg) | NaOL/FeOL[b)] | OA (μL) | Temperature (°C) | Products[c)] |
|---|---|---|---|---|---|---|
| ODE | 900 | 30 | 1:10 | 160 | Reflux | |
| ODE | 900 | 60 | 2:10 | 160 | Reflux | |
| ODE | 900 | 180 | 6:10 | 160 | Reflux | |
| TOA | 900 | 0-30 | 0-1:10 | 160 | 340 | |
| TOA | 900 | 60 | 2:10 | 160 | 340 | |
| TOA | 900 | 150 | 5:10 | 160 | Reflux | |
| TOA | 450 | 15 | 1:10 | 80 | Reflux | |

[a]The volume of solvent was 15 mL. [b]Represents the molar ratio of NaOL and FeOL. [c]The cube represents a 21 nm sized IO cube. [d]Reprinted (adapted) with permission from ref 26. Copyright 2015 American Chemical Society

chlorides (sodium chloride and potassium chloride) to yield octahedra (111) faceted MgO particles.[8] It was found that utilizing magnesium nitrate hexahydrate or magnesium chloride hexahydrate was the only oxide precursors to yield (111) facets during the molten salt procedure; however, magnesium acetate hexahydrate, magnesium hydroxide, magnesium oxalate dihydrate, hydromagnesite, and magnesium oxide were also studied as oxide precursors but were not successful in (111) facet exposure. SEM images of the products can be found in Figure 20.

All calcinations in air with molten salts were performed with alumina crucibles in a muffle furnace. Samples were prepared by mixing the powder in the appropriate proportions as described below and grinding them with a mortar and pestle. After the calcination step, the salts are washed off by deionized water, followed by suction-filtration and washing with deionized water and ethanol and dried overnight at 50 °C.

When using a molten nitrate medium, a 10–30 wt % of either magnesium nitrate hexahydrate or magnesium chloride hexahydrate can be utilized. Using lithium nitrate as the molten medium, a


https://doi.org/10.1021/acs.cgd.2c00409
Cryst. Growth Des. 2022, 22, 6296–6322

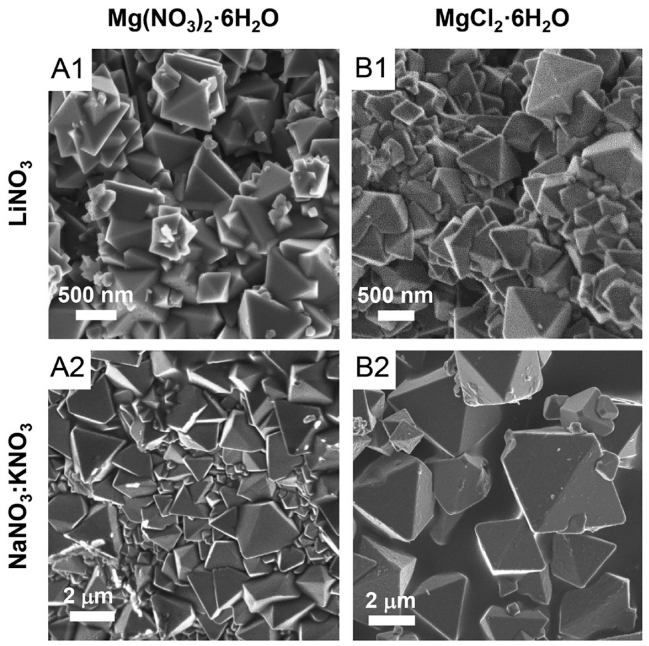


**Figure 20.** SEM of MgO produced by thermal decomposition of 10 wt % precursor mixtures at 500 °C where letters (columns) refer to precursors and numbers (rows) refer to the salt media: (A) $Mg(NO_3)_2 \cdot 6H_2O$ and (B) $MgCl_2 \cdot 6H_2O$ in (1) $LiNO_3$ for 5 h, and in (2) $NaNO_3$:$KNO_3$ (3:2) for 10 h. Heating rates: 2.5 °C/min. Reprinted (adapted) with permission from ref 8. Copyright 2018 American Chemical Society.

calcination temperature of 500 °C for 5 h at a ramp rate of 2.5 °C/min is used.

When utilizing a molten chloride medium such as sodium chloride: potassium chloride, a (1:1) ratio was used with 30 wt % of magnesium nitrate hexahydrate as the oxide precursor. Calcination parameters utilized were 550 °C for 2 h at a ramp rate of 2.5 °C/min.

It was found that the decomposition trajectory of the oxide precursor, magnesium nitrate hexahydrate, is important for the formation of the (111) facet, and schematics can be found in Figures 21, 22, and 23. The decomposition trajectory can be controlled by using specific heating profiles, regulated atmospheres, or by the addition of specific salts in a reaction mixture. Interestingly, the decomposition of magnesium nitrate hexahydrate in the absence of additional salts (neat system) is shown in Figure 21. An important finding here is that when water-free air was utilized, the products yielded ill-defined morphologies, whereas using normal laboratory air (wet air) yielded defined octahedral (111) faceted morphologies. Therefore, MgO(111) facets were promoted via magnesium nitrate intermediates in the molten state and with the presence of residual water. A table of content (TOC) image of the whole process is provided in Figure 24.[8]

In a molten nitrate environment, the creation of liquid eutectic mixtures helps preserve water and ionic mobility resulting in the formation and stabilization of the (111) facet. This finding again emphasizes the important role water has. However, in a eutectic chloride environment and without the presence of water, MgO formation is most likely to happen before bulk melting of the chloride salt combination. It is speculated that the intermediate, $K_3NaMgCl_6$, might locally melt, and this intermediate provides a pathway toward the final MgO product. The (111) facet stabilization may occur via the adsorption of $K^+/Cl^-$ ions on the (111) facet or by addition of specific growth units ($Mg^{2+}$-chloride complexes).[8]

It is important to highlight that it has previously been hypothesized that strong electrostatic interactions between the free ions in the molten medium and the polar (high surface energy) facets of the oxide products possibly lower the surface energy of the MgO(111), which results in slower growth rates and an increase of these facets.[5,7,85]

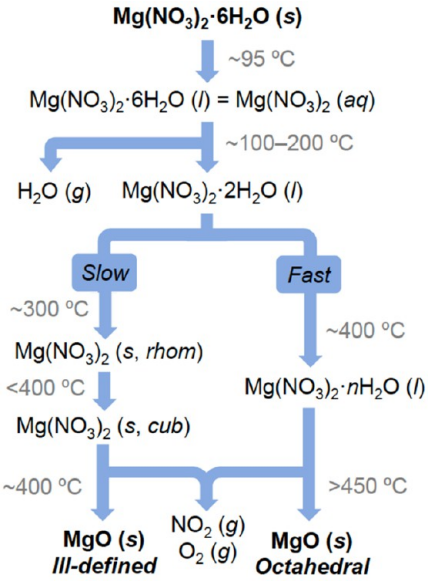


**Figure 21.** Proposed schematic of $Mg(NO_3)_2 \cdot 6H_2O$ thermal decomposition pathways in air (based on PXRD measured at RT). Reprinted (adapted) with permission from ref 8. Copyright 2018 American Chemical Society.

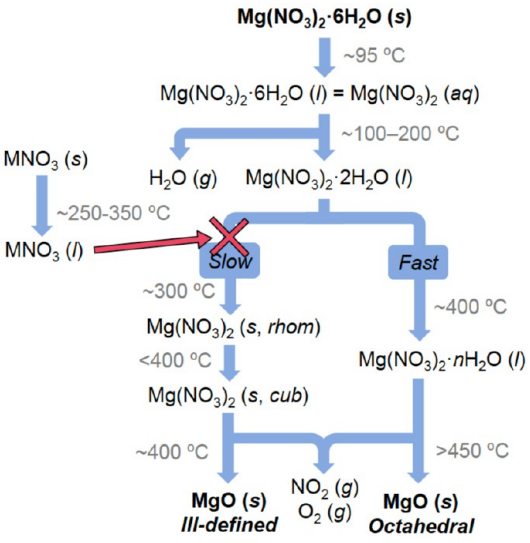


**Figure 22.** Proposed schematic decomposition pathway in molten nitrate media for $Mg(NO_3)_2 \cdot 6H_2O$. In nitrate-based systems, eutectic mixtures ensure the liquid state of the reaction mixture, favoring a liquid-to-solid mechanism for the formation of MgO. Reprinted (adapted) with permission from ref 8. Copyright 2018 American Chemical Society.

In a summary of this case study, the molten salt medium is speculated to adsorb and to stabilize specific crystal facets, in this case the (111) facet, in situ or face dissolution−recrystallization processes.[8] In the chloride salt system, the formation of the intermediate $K_3NaMgCl_6$ is necessary for the conversion to MgO. While some experiments here indicated that the presence of water was important, its exact role is still unknown. Overall, the choice of salts, metal precursors, calcination temperature, ramp, rate, and atmosphere all contributed to the formation and stabilization of the (111) facet.

*2.2.3. NiO(111) Octahedral Particles.* Nickel oxide (111) octahedral particles were synthesized by Susman et al.[25] To start, nickel nitrate hexahydrate as the metal precursor and lithium nitrate as the molten salt in a 1:10 molar ratio of precursor:salt were ground using a mortar and


https://doi.org/10.1021/acs.cgd.2c00409
Cryst. Growth Des. 2022, 22, 6296−6322

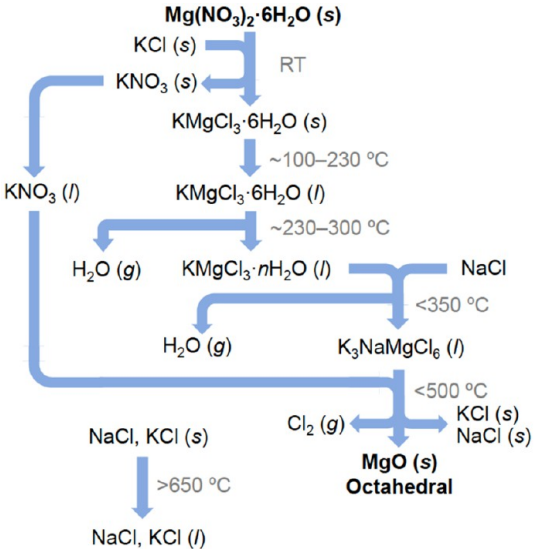


**Figure 23.** Proposed schematic of $Mg(NO_3)_2{\cdot}6H_2O$ thermal decomposition pathway in NaCl:KCl (1:1). Reprinted (adapted) with permission from ref 8. Copyright 2018 American Chemical Society.

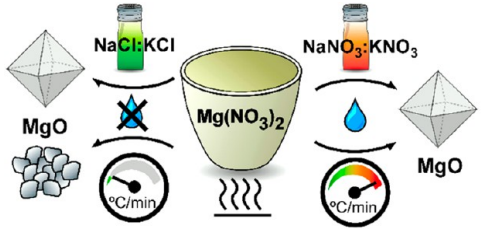


**Figure 24.** Table of content reprinted (adapted) with permission from ref 8. Copyright 2018 American Chemical Society.

pestle. The calcination parameters used were 550 °C at a heating rate of 2.5 °C/min. After calcination, samples were washed with deionized water and ethanol and dried at 50 °C. Additionally, NiO(111) octahedral particles can form through direct thermal decomposition of nickel nitrate hexahydrate in air.[25,86] Images of the products calcined with the salt and in the absence of salt can be seen in Figure 25. The authors speculated that the growth pathway and final (111) faceting are associated with the coordination number of $Ni^{2+}$ species.[25]

*2.2.4. $LaCoO_3$ (111) and $La_xSr_{1-x}CoO_3$ (111).* Microcrystalline perovskite cobaltite samples of $LaCoO_3$ (111) and $La_{0.7}Sr_{0.3}CoO_3$ (111) with enhanced CO oxidation activity were synthesized by Wang et al. via the molten salt route.[6]

$LaCoO_3$ (111) was synthesized by mixing 1.7 mmol of lanthanum-(III) nitrate hexahydrate, 0.5 mmol strontium nitrate, 2 mmol of cobalt(II) nitrate hexahydrate, and 120 mmol of potassium chloride:sodium chloride molten salt medium in a (1:1) ratio in a mortar and ground to a fine powder. The mixture is then transferred to a crucible and calcined in air at 750 °C for 2 h at a ramp rate of 5 °C/min. After being cooled to room temperature, hot deionized water is added to the crucible and sonicated. The samples are then filtered and repeatedly washed with deionized water until no remaining $Cl^-$ ions are left. To remove any mixed phases of strontium carbonate, a further washing with dilute acid is performed. The samples are the dried at 60 °C overnight in air.

$La_{0.7}Sr_{0.3}CoO_3$ (111) was synthesized in a similar fashion except with different starting amounts of oxide precursors. 1.2 mmol of lanthanum-(III) nitrate hexahydrate, 1.2 mmol strontium nitrate, 2 mmol of cobalt(II) nitrate hexahydrate, and 120 mmol of potassium chloride:sodium chloride molten salt medium in a (1:1) ratio were mixed and ground in a mortar and transferred to a crucible. The calcination temperature this time was 800 °C for 2 h at a ramp rate of 5 °C/min. The same washing and drying treatments were performed on these samples as well.

Reasons governing the (111) facet exposure included slowing the growth rate of the (111) facet by introducing small amounts of strontium ions. They reported that the $Cl^-$ and $Sr^{2+}$ ions in the molten salt have a strong interaction with the exposed crystal facet of the perovskite cobaltite materials, and changing the strontium concentration in the sodium chloride:potassium chloride molten salt medium can tune the surface energy and growth rate of the crystal facets resulting in the desired high energy (111) facet.[6] A brief schematic of the molten salt process and TEM image can be found in Figure 26 and Figure 27 respectively. Additionally, Figure 28 shows SEM images depicting facet formation with varying strontium doping percentages as well as varying temperatures.

**2.3. Topochemical Conversion Method.** Topochemical or topotactic conversion is a reaction that introduces/removes guest species into/from a host structure thereby resulting in a structurally similar structure with a significant composition difference to the host structure. This strategy is commonly used for metal hydroxide−oxide conversion to yield oxide surfaces or layers with well-defined orientation.[87,88] Recently, topotactic conversion has emerged as a method to produce 2D ultrathin nanosheets by surface modification, heat treatment, nitrogenization, and molecules/ions intercalation of/into a layered precursor.[21,89−92]

*2.3.1. $Co_3O_4$(111) Atomically Thin Nanosheets.* Zhu et al. utilized a topochemical transformation route to convert a few layers of alpha-cobalt(II) hydroxide ($\alpha$-$Co(OH)_2$) into atomically thin $Co_3O_4$ nanosheets (ATCN's).[18]

There are two main steps: one is the formation of $\alpha$-$Co(OH)_2$, and the other is the transformation of $\alpha$-$Co(OH)_2$ into ATCN. Few-layer thick precursor nanosheets of $\alpha$-$Co(OH)_2$ are made by combining a cobalt chloride solution to ethylene glycol to reach a $Co^{2+}$ concentration of 1.5 mM. Ammonia is then slowly dropped to the stirring solution until a pH of about 9.5 is reached before transfer to a Teflon-lined stainless-steel autoclave. The autoclave is then heated in an electric oven at 130 °C for 24 h. After the product is cooled down, the resulting green cobalt hydroxide precursor is filtered and washed with distilled water and ethanol several times and added into a bottle and sonicated for 6 h. Centrifugation at 4000 rpm for 5 min yields resultant dispersions that become transparent, and the supernatant is collected at high centrifugation speeds. The obtained sample is then dried at 60 °C under a vacuum overnight.

To yield ATCNs, the prepared $\alpha$-$Co(OH)_2$ precursor nanosheets are added into ethanol to form a colloidal suspension followed by the addition of hydrogen peroxide solution into the suspension at 60 °C for 4 h. To remove any lingering nanoparticles after topotactic conversion, the dispersions are centrifuged at 2000 rpm for 20 min. After this, the supernatant is collected by centrifuging the mixture yet again at 12 000 rpm for 5 min and dried under a vacuum overnight. A general schematic of the process can be seen in Figure 29.

Unlike the case studies written above where a specific synthetic parameter affects the facet outcome, here the authors describe a transformation that is enabled by the structural similarity between $Co(OH)_2$ and $Co_3O_4$. The lattice spacings between the (100) facets of $Co(OH)_2$ and the (200) facets of $Co_3O_4$ are calculated to be below 3% indicating a close lattice match.[18] More importantly, the $Co^{2+}$ atomic structures of the (001) plane of $Co(OH)_2$ and the (111) plane of $Co_3O_4$ have the same symmetry (Figure 29b). The structural similarity between $Co(OH)_2$ and $Co_3O_4$ ultimately facilitates the development of (111) faceted ATCN's from the (001)-faceted $\alpha$-$Co(OH)_2$ nanosheets.[15,18]

*2.3.2. MgO(111) 2D-Nanosheets.* Similar to the synthesis of atomically thin $Co_3O_4$ nanosheets (ATCN's) described above, MgO(111) ultrathin nanosheets can also be formed via topotactic conversion.[21] The synthesis consisted of three steps: production of high surface area oxide nanoparticles, hydrolysis of the nanoparticles to form hydroxylated nanosheets, and decomposition back to the oxide form via topotactic conversion.


https://doi.org/10.1021/acs.cgd.2c00409
Cryst. Growth Des. 2022, 22, 6296−6322

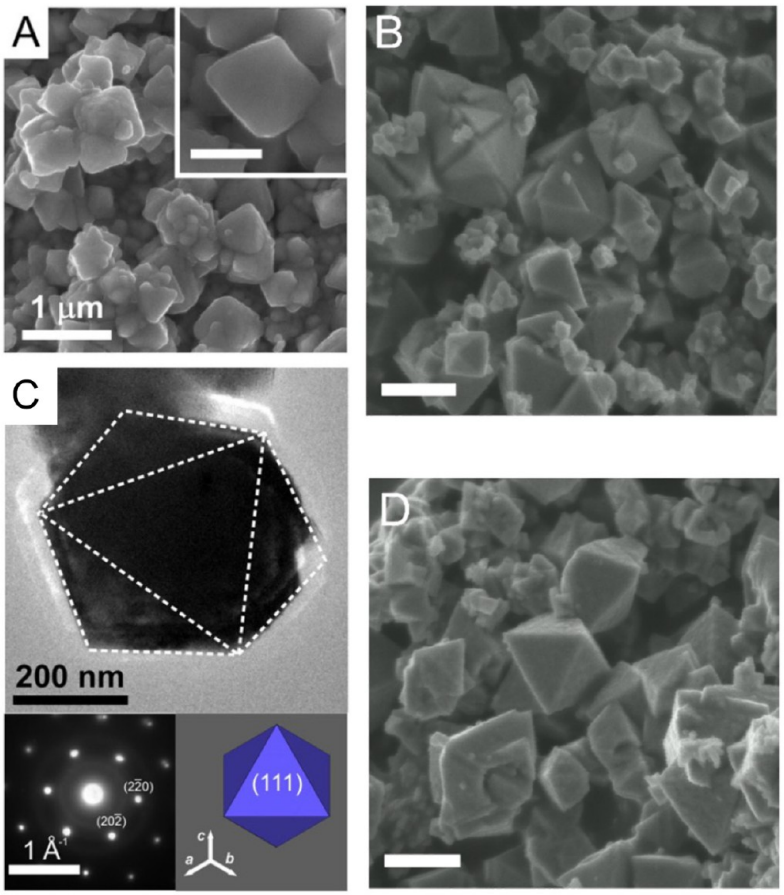


**Figure 25.** (A) Scanning electron microscopy (SEM) and (C) transmission electron microscopy (TEM) of NiO particles produced by molten salt synthesis in $LiNO_3$. (B, D) SEM images of NiO produced at 20 °C/min at 500 and 2.5 °C/min at 350 °C respectively in air. Scale bars: 400 nm. Reprinted (adapted) with permission from ref 25. Copyright 2020 John Wiley & Sons.

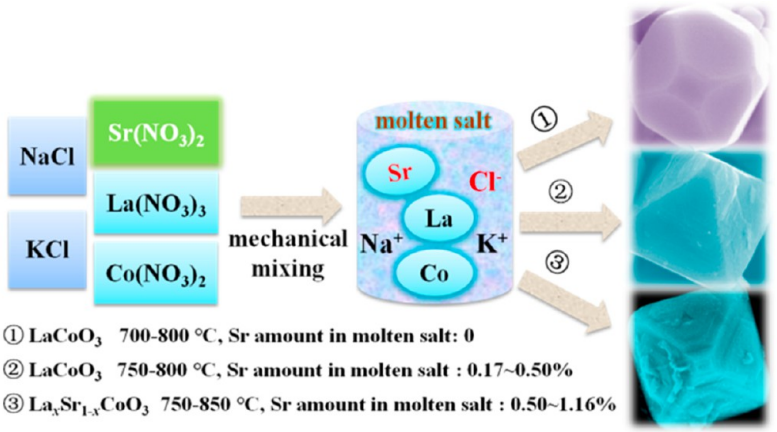


**Figure 26.** Scheme of the molten salt flux synthetic route of perovskite cobaltite with different crystal facets and surface morphologies measured in SEM for $LaCoO_3$ (110 and 100), $LaCoO_3$ (111), and $La_{0.7}Sr_{0.3}CoO_3$ (111). Reprinted (adapted) with permission from ref 6. Copyright 2018 American Chemical Society.

To produce high surface area MgO nanoparticles (MgO-p), a sodium carbonate aqueous solution is added into a magnesium nitrate hexahydrate aqueous solution under stirring at room temperature for 10 min. Afterward, the precipitate is collected by filtration, washed with deionized water and ethanol, and dried under reduced pressure. The powder was then calcined at 500 °C for 2 h in air with a ramp rate of 2 °C/min.

The nanoparticles synthesized above are then added into deionized water (1 mg/mL) under stirring for 1 h. The product is then collected through filtration and dried under reduced pressure yielding magnesium hydroxide nanosheets.

To obtain ultrathin 2D MgO(111) nanosheets (MgO-NS), the magnesium hydroxide nanosheets created via the hydrolysis step above are then subjected to calcination under high vacuum. The heat treatment required the reactor to be evacuated with a pressure lower than $10^{-5}$ mbar during both ramping and heating phases. The nanosheets are heated at 600 °C for 12 h and stored under argon afterward. Images of the products can be seen in Figure 30.



https://doi.org/10.1021/acs.cgd.2c00409
Cryst. Growth Des. 2022, 22, 6296−6322

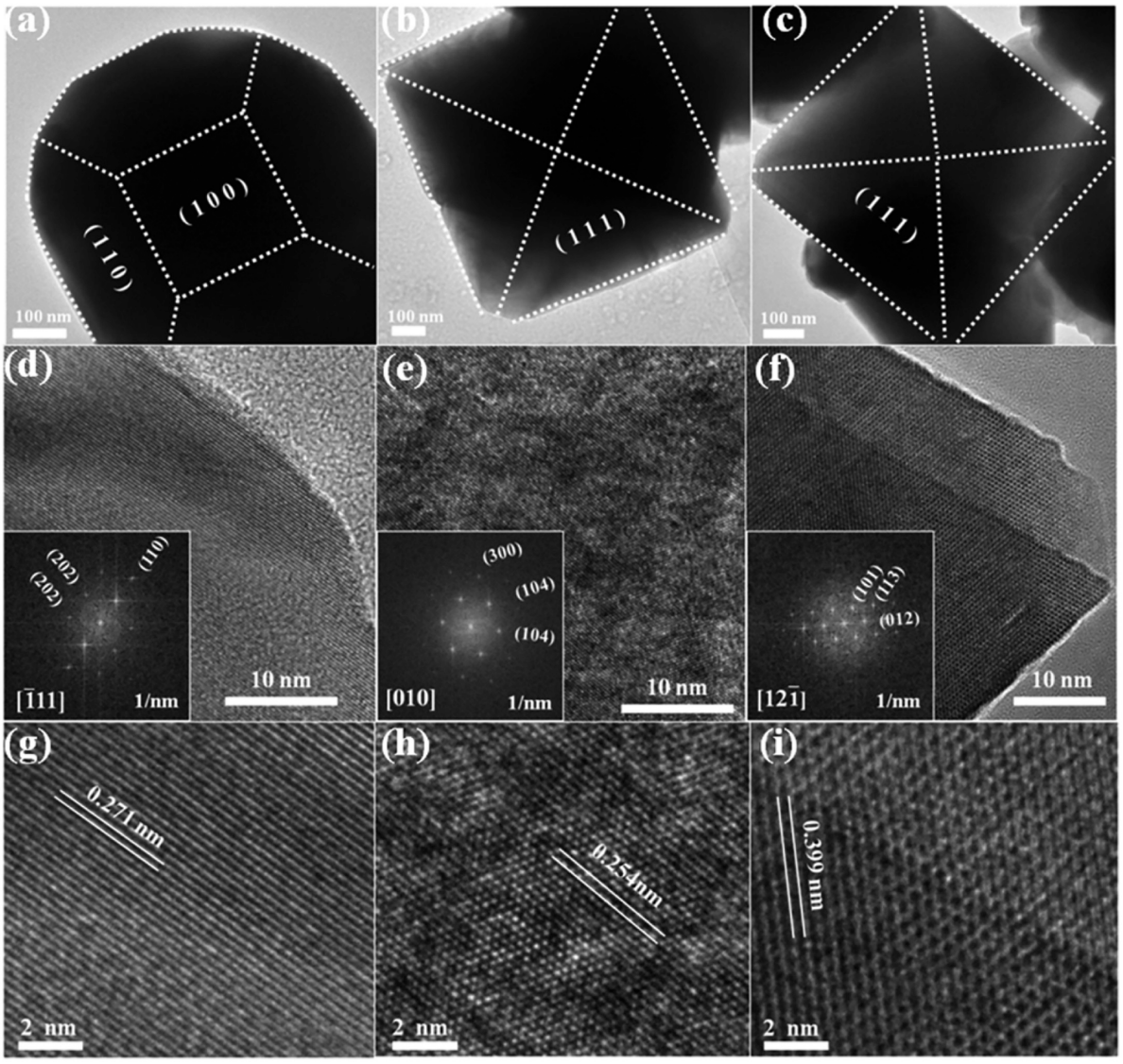


**Figure 27.** Bright-field TEM images of (a) $LaCoO_3$ (110 and 100), (b) $LaCoO_3$ (111), and (c) $La_{0.7}Sr_{0.3}CoO_3$ (111). The corresponding fast Fourier transform (FFT) patterns of (d) $LaCoO_3$ (110 and 100), (d–f) electron diffraction patterns, (e) $LaCoO_3$ (111), and (f) $La_{0.7}Sr_{0.3}CoO_3$ (111). High-resolution TEM images for (g) $LaCoO_3$ (110 and 100), (h) $LaCoO_3$ (111), and (i) $La_{0.7}Sr_{0.3}CoO_3$ (111). Reprinted (adapted) with permission from ref 6. Copyright 2018 American Chemical Society.

It was concluded that the ultrathin 2D-MgO(111) was made possible only using dynamic heating under a vacuum. For reference, when hydroxide nanosheets were heat treated under $N_2$ flow, they decomposed into polycrystalline MgO instead of single-crystalline MgO. Therefore, the dynamic heating under a vacuum made it possible to remove the produced water, thus preventing the reversibility of the topotactic reaction $Mg(OH)_2 \rightleftharpoons MgO + H_2O$ and safeguarding the conversion to single-crystalline ultrathin 2D MgO(111) nanosheets.[21]

**2.4. Solution Combustion Method.** The solution combustion method was developed during the 1980s, is relatively simple to execute, and is utilized in the synthesis of nanomaterials, metal oxides, metals, alloys, and sulfides. This method starts with dehydration and thermal decomposition of a homogeneous solution and involves several thermally coupled exothermic reactions that result in the formation of a solid product and a large amount of gases. This process typically uses an oxidizer, organic fuel, and a solvent.[93]

*2.4.1. MgO(111).* Hao et al. synthesized MgO (111) with a surface area of 7.08 $m^2/g$ by a high temperature solution combustion method.[22] To start, 0.010 mol of magnesium nitrate hexahydrate and 0.020 mol of urea were mixed. The mixture was then heated in an electric furnace until complete combustion.

The main reason for the (111) facet exposure in this case study was speculated to be due to the combustion atmosphere being in a reduced state caused by the excess of fuels. The authors stated that the oxygen atoms of the MgO(111) would release thereby leaving surface oxygen vacancies. This can be expressed by the following reaction: $O_o = \ddot{V}_o + \frac{1}{2}O_2(g) + 2e^-$. The whole MgO solution combustion process is described by this reaction: $Mg(NO_3)_2 \cdot 6H_2O(s) + 2CO(NH_2)_2(s) + 0.5O_2(g) \xrightarrow{\Delta} MgO(s) + 2CO_2(g) + 3N_2(g) + 10H_2O(g)$[22] and facet model can be seen in Figure 31 and Figure 32 respectively.

**2.5. One-Pot Assembly Method.** The one-pot synthesis method is most ideal to synthetic chemists in terms of simplicity and resources. It is a strategy that can improve the efficiency of chemical reactions that occur during synthesis utilizing just one reactor.

*2.5.1. $Cu_2O$(111) Nanospheres.* Cuprous oxide is a p-type semiconductor and has meaningful applications in antibacterial activity, photocatalysis, gas sensors, chemical template, solar-driven water splitting, among others.[27]



https://doi.org/10.1021/acs.cgd.2c00409
Cryst. Growth Des. 2022, 22, 6296–6322

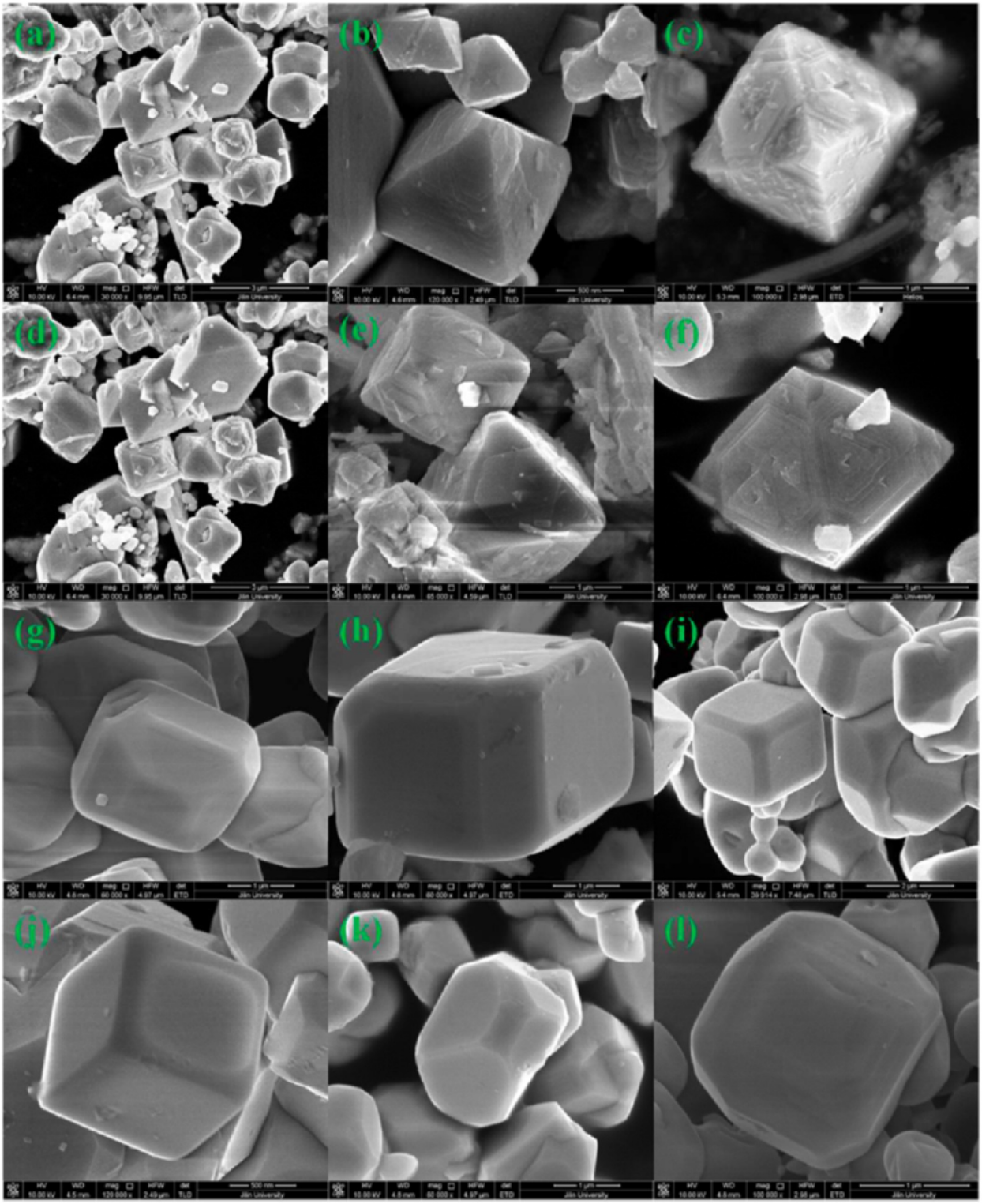


**Figure 28.** SEM image of (a) $LaCoO_3$ (111) at 750 °C with 0.30% Sr, (b) $LaCoO_3$ (111) at 800 °C with 0.30% Sr, (c) $LaCoO_3$ (111) at 800 °C with 0.17% Sr, (d) $La_xSr_{1-x}CoO_3$ (111) at 800 °C with 0.50% Sr, (e) $La_xSr_{1-x}CoO_3$ (111) at 800 °C with 1.00% Sr, (f) $La_xSr_{1-x}CoO_3$ (111) at 800 °C with 1.16% Sr, (g) $LaCoO_3$ (110 and 100) at 700 °C, (h) $LaCoO_3$ (110 and 100) at 750 °C, (i) $LaCoO_3$ (110 and 100) at 800 °C, (j) $LaCoO_3$ (110 and 100) at 750 °C in NaCl molten salt, (k) $LaCoO_3$ (110 and 100) at 750 °C in KCl molten salt, (l) $LaCoO_3$ (110 and 100) at 750 °C in 180 mmol of NaCl-KCl molten salt. (a−f) Unmarked conditions are at 800 °C for 5 h in 120 mmol KCl-NaCl (1:1) molten salts at 5 °C/min, $g^{-1}$: unmarked conditions are at 750 °C for 5 h in 120 mmol KCl-NaCl (1:1) molten salts at 5 °C/min. Reprinted (adapted) with permission from ref 6. Copyright 2018 American Chemical Society.

Sun et al. synthesized $Cu_2O$(111) nanospheres with enhanced photochemical activities via a quick and easy one-pot assembly system with the help of an additive-assisted complex-precursor solution.[27] To start, copper(II) acetate and b-cyclodextrin (b-CD) are dissolved in



https://doi.org/10.1021/acs.cgd.2c00409
Cryst. Growth Des. 2022, 22, 6296−6322

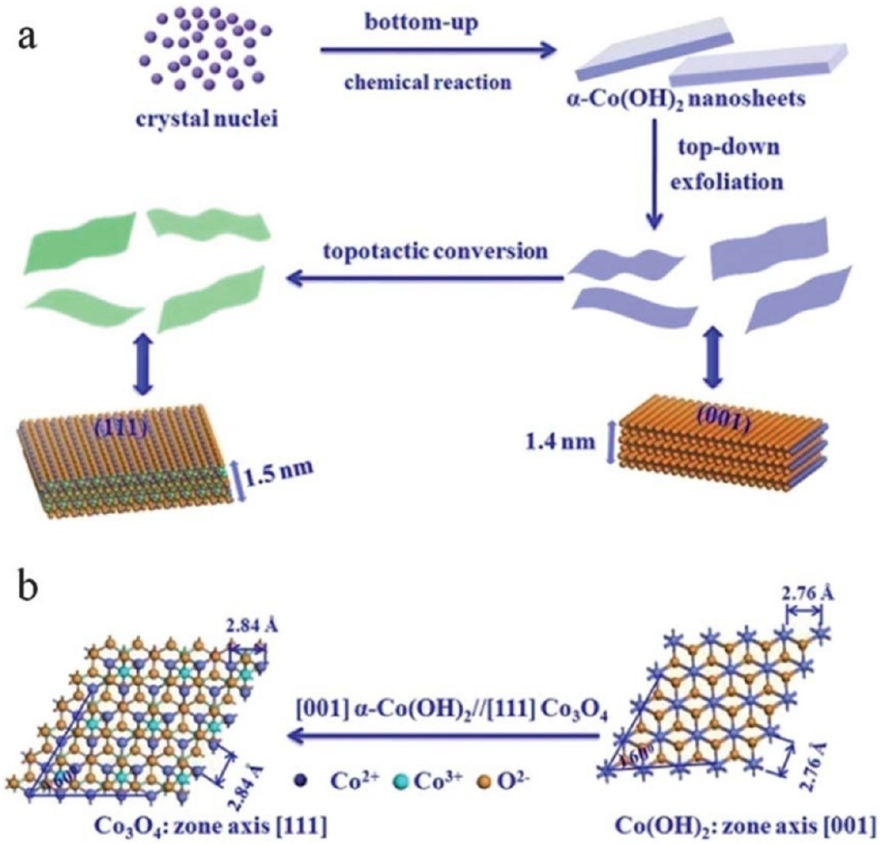


**Figure 29.** (a) Schematic illustration of the preparation of ATCNs. (b) Schematic model of the top-view illustrating the topochemical transformation from the $Co(OH)_2(001)$ plane to the $Co_3O_4$ (111) plane. The highly oriented growth of the ATCNs is attributed to $\alpha$-$Co(OH)_2$-to-$Co_3O_4$ topochemical conversion, with the relationship of [001] a-$Co(OH)_2$//[111] $Co_3O_4$. Reprinted (adapted) with permission from ref 18. Copyright 2013 Royal Society of Chemistry.

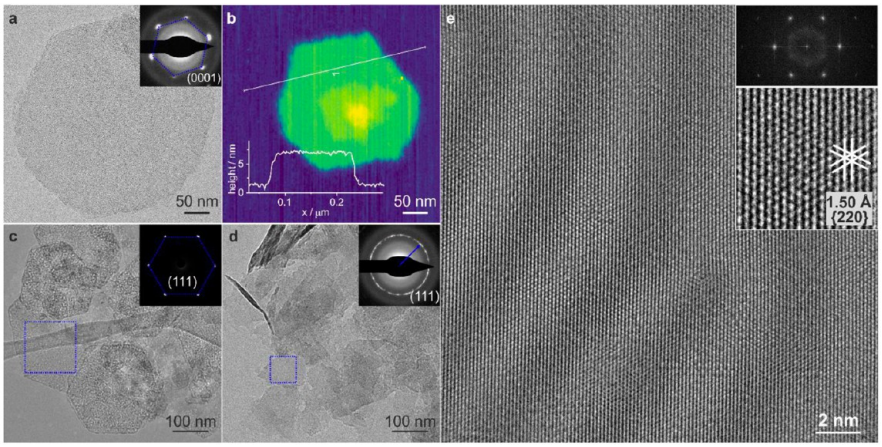


**Figure 30.** Characterization of $Mg(OH)_2$ nanosheets and MgO nanosheets. Representative TEM images and SAED patterns of (a) a freestanding $Mg(OH)_2$ nanosheet from the (0001) direction, (c) MgO-NS and (d) MgO-p. (b) AFM image of a single $Mg(OH)_2$ nanosheet with sub-monolayer attachment and corresponding thickness along the line. (e) HRTEM image of MgO-NS; insets are the fast Fourier transform (FFT) pattern and enlarged image showing the (220) lattice fringes. Reprinted (adapted) with permission from ref 21. Copyright 2021 John Wiley and Sons.

ultrapure water and stirred at 55 °C for 5 min. Next, anhydrous ethanol (EtOH) was added into the solution causing a decrease in solution temperature. Once the temperature reached 55 °C again, a sodium hydroxide (NaOH) solution is added dropwise to the $Cu^{2+}$/b-CD/$EtOH/H_2O$ mother solution. A precipitate then forms slowly and is stirred for 5 min before adding D-(+)-glucose powder and stirred for another 5 min at 60 °C. This one-pot process yields a yellow precipitate that is separated by centrifugation, washed with ultrapure water and ethanol, and dried at 50 °C for 60 min in a vacuum oven. Results of the product are seen in Figure 33.

Factors for the (111) facet formation on $Cu_2O$ in this one-pot assembly can be attributed to the synergic effect of nanoparticle aggregation and ripening with facet-selective adsorption. Sun et al. proposed that the presence of hydroxyls sourced from ethanol molecules helps protect the planes of the $Cu_2O$ nanoparticle building blocks, which in turn delays the aggregation and ripening process to


https://doi.org/10.1021/acs.cgd.2c00409
Cryst. Growth Des. 2022, 22, 6296−6322

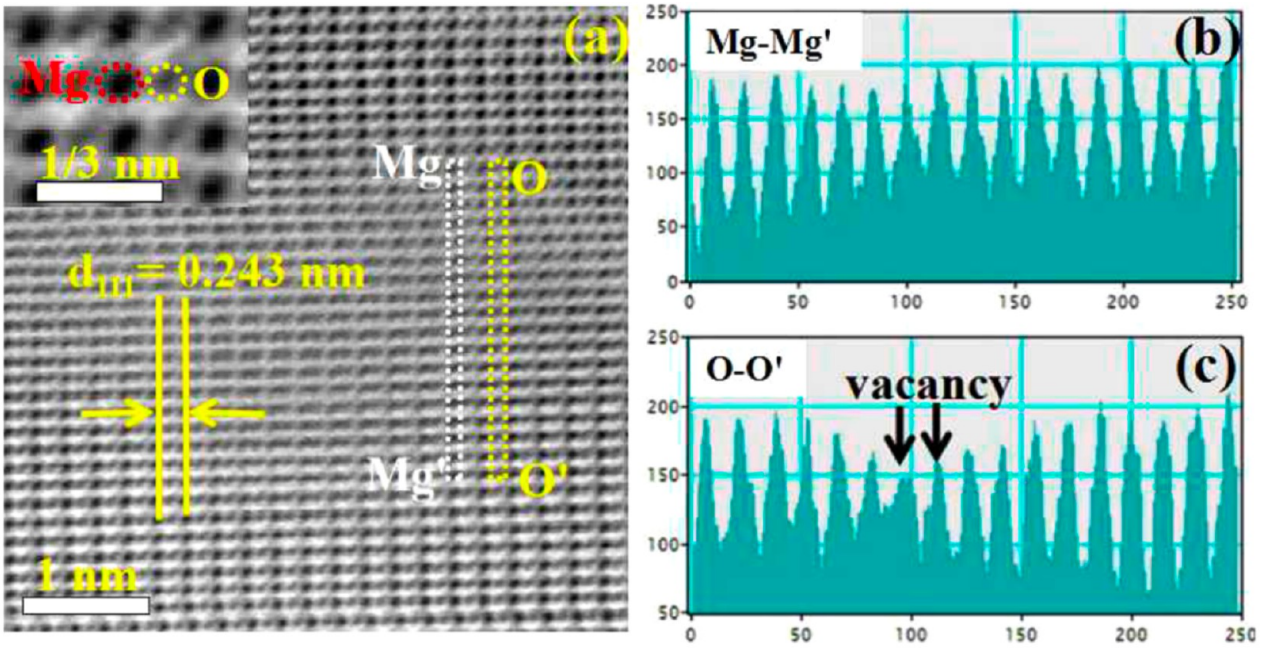


**Figure 31.** (a) Aberration-corrected annular bright-field image of the as obtained MgO and line profiles of Mg (b) and O (c) atoms along the vertical direction with regard to the dotted lines of panel a, showing the atom intensity versus position. Reprinted (adapted) with permission from ref 22. Copyright 2017 American Chemical Society.

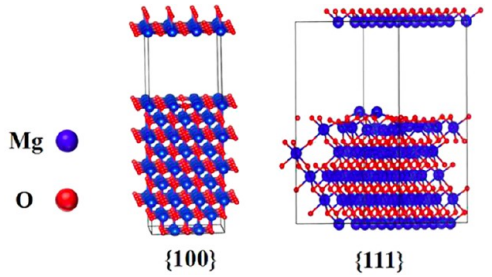


**Figure 32.** Tilted side views of 2 × 2 × 1 supercell of MgO (100) and (111) facets with one oxygen vacancy. Reprinted (adapted) with permission from ref 22. Copyright 2017 American Chemical Society.

minimize the total free energy of the system and yield $Cu_2O$(111) nanospheres.[27]

*2.5.2. $Cu_2O$(111) Microcrystals.* Li et al. synthesized $Cu_2O$ (111) microcrystals by a facile glucose reduction method in a one-pot assembly.[28] They started off by mixing a certain amount of polyvinylpyrrolidone (PVP) and 0.171 g of copper chloride in 100 mL aqueous solution to create a desired "*r*" ratio. Here the "*r*" ratio is the molar ratio of PVP and copper salt. The solution is then stirred for 30 min followed by the quick addition of a sodium hydroxide solution and heated to 80 °C. Once the solution reached 80 °C, glucose is slowly added dropwise, and the assembly is kept in a water bath at a temperature of 80 °C for 2 h and allows to cool to room temperature. This yields a brick red precipitate that is centrifuged, washed with distilled water and absolute alcohol, and dried in an oven at 60 °C for 5 h.

It was found that with an increase in PVP concentration, the proportion of (111) facets became abundant, while the (100) planes decreased as depicted in Figure 34−35. Since PVP is a stabilizing agent, Li et al. claimed that PVP molecules are polarized to create a (−C═O) functional group that adsorbs on the surface of $Cu_2O$ particles via physical and chemical bonding.[28] Thus, when PVP is added to the reaction mixture, it is speculated that PVP can slow the growth of the (111) facets more than that of the (100) planes due to unsaturated $Cu^{2+}$ on the surface of the (111) facets.[28] An image of the (111) surface structure is provided in Figure 36.

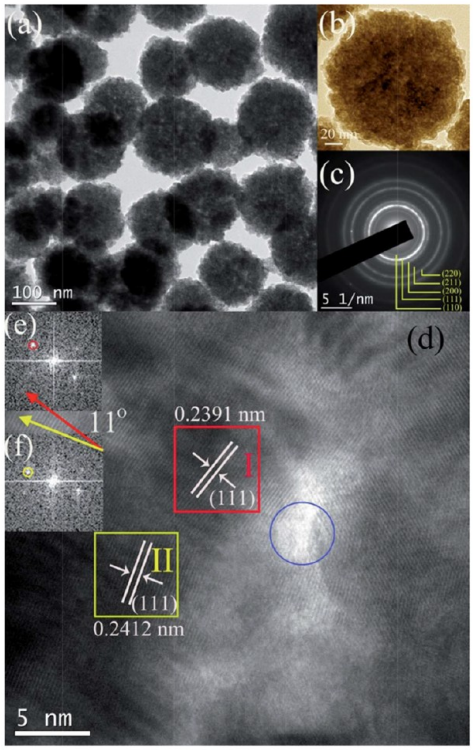


**Figure 33.** (a) Low-magnification TEM image of as-prepared hierarchical $Cu_2O$ nanospheres; (b) An individual hierarchical $Cu_2O$ nanosphere; (c) the corresponding SAED pattern of the particle as shown in Figure 2b; (d) HRTEM image of the hierarchical $Cu_2O$ nanosphere; (e) and (f) FFT images taken from the areas marked with red and yellow squares in Figure 33d, respectively. Reprinted (adapted) with permission from ref 27. Copyright 2012 Royal Society of Chemistry.



https://doi.org/10.1021/acs.cgd.2c00409
Cryst. Growth Des. 2022, 22, 6296−6322

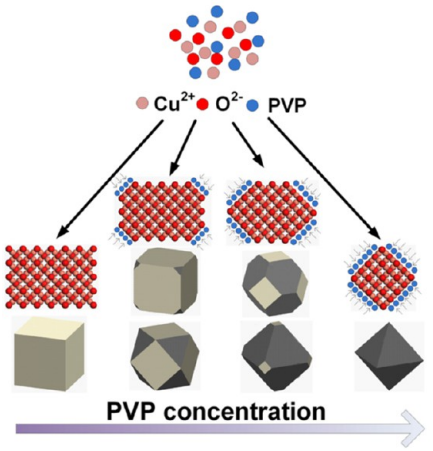


**Figure 34.** Schematic of the crystal growth mechanism. Reprinted (adapted) with permission from ref 28. Copyright 2015, Springer Science Business Media New York.

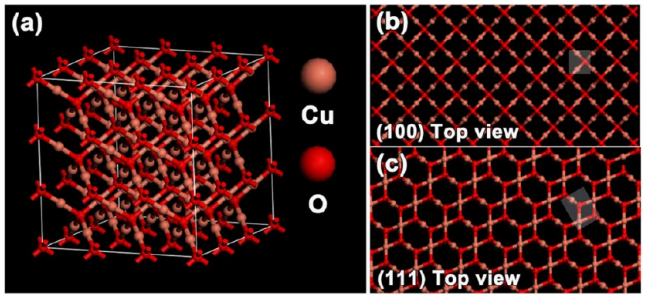


**Figure 36.** (a) Supercell structures of $Cu_2O$; (b) side view of the $Cu_2O$ (100) surface; (c) side view of the $Cu_2O$ (111) surface. The shaded areas represent the periodic unit of (100) surface and (111) surface, respectively. Reprinted (adapted) with permission from ref 28. Copyright 2015, Springer Science Business Media New York.

## 3. GOVERNING SYNTHETIC PARAMETERS

Taken together, the recurring theme linking these syntheses is the need to either lower the surface energy of the unconventional (111) facet or to block the pathways that could otherwise enable the formation of other facets. Selection of directing

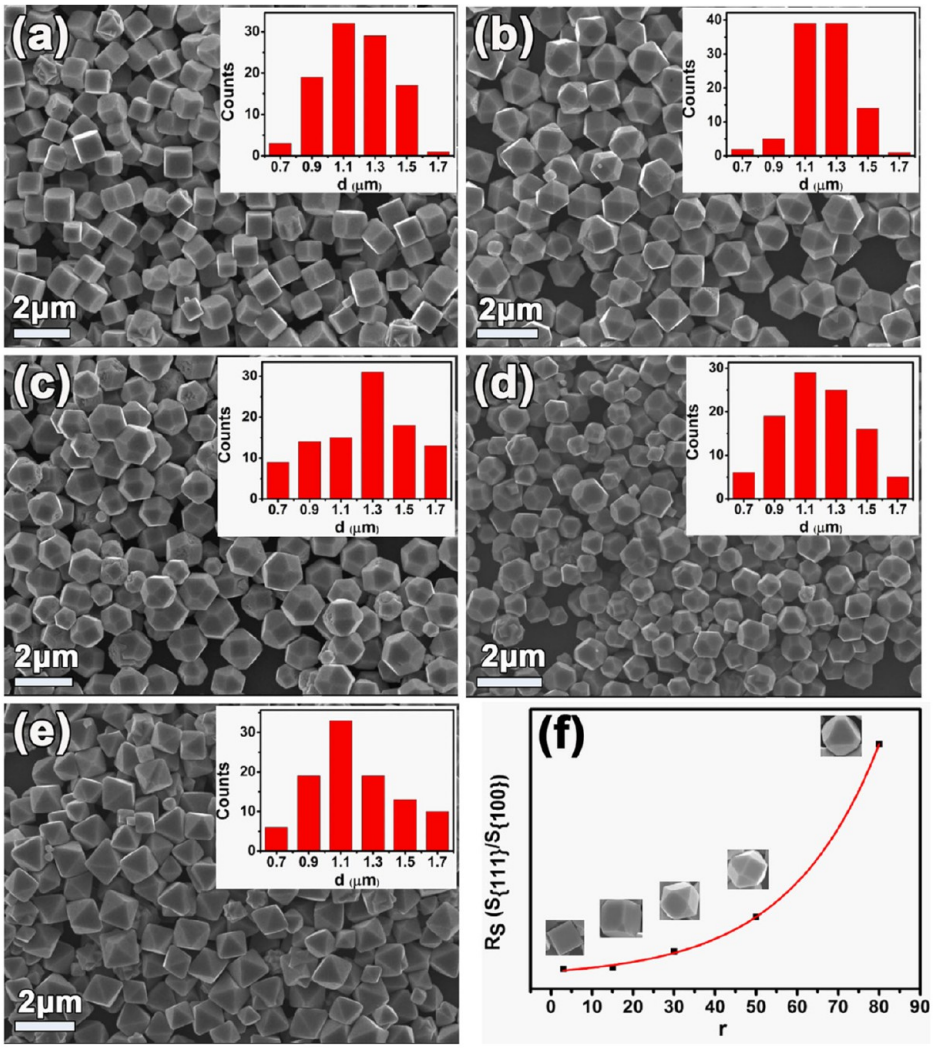


**Figure 35.** Typical FESEM images and the size distribution diagram of other five morphologies of $Cu_2O$: (a) $r$ = 15:1; (b) $r$ = 30:1; (c) $r$ = 50:1; (d) $r$ = 80:1; (e) $r$ = 100:1; (f) the area ratio curve of (111) and (100) along with different '$r$' ratios. Reprinted (adapted) with permission from ref 28. Copyright 2015, Springer Science Business Media New York.



https://doi.org/10.1021/acs.cgd.2c00409
Cryst. Growth Des. 2022, 22, 6296−6322

agents, precursors, and reactants, as well as the conditions in which they are mixed in solution (temperature, pH etc.) directly affect the surface energy to the point that they can lower it enough to become the most favorable surface.

For the hydrothermal/solvothermal synthetic methods, careful selection of reagents, solvents, structure directing agents, metal precursors, and intermediates, along with specific concentrations, leads to (111) facet formation. Additionally, temperature, pH, and the presence of residual water had a role in forming the (111) facet.

Similarly, for the thermo-decompostion methods, the (111) facet exposure relied on the synthetic parameters of selection of reagents and solvents, molar ratio, metal precursor and intermediates, selection of molten salt media, and atmosphere conditions.

In the topotactic transformations that lead to (111) nanosheets, the presence of hydroxides as precursors that *already* have the correct surface orientation will enable the formation of the (111) simply by eliminating water: when starting from hydroxides, the pathways to any other orientations than (111) are effectively blocked.[15,18,21] These precursors all but ensure that there are virtually no pathways toward creating surfaces or nanosheets with any other orientation than (111). Control over their crystallinity and thickness was also enabled by the removal of water produced under a vacuum, so that the topotactical transformation proceeds only in the direction of forming (111) oxide nanosheets.

As for the solution combustion method, the (111) facet exposure for MgO(111) relied on a reductive atmosphere during combustion thereby falling under the synthetic category of atmospheric condition.

For the one-pot assembly method, the (111) facet exposure relied on the selection of reagents and solvents as well as the molar ratio.

## 4. APPLICATIONS

The applications of (111) faceted metal oxides are vast and cover a variety of relevant industrial and environmental applications. To reiterate, naturally exposed surfaces are usually stable and chemically less active; therefore, exposing the facets of high-index facets with high surface energies may exhibit enhanced chemical properties.[5] The (111) facet may not always have superior performance in the scenario that it is a crystal structure's most stable facet naturally. However, much of this review focuses on metal oxide crystal structures that do not naturally form (111) facets and thus will have enhanced performance in a variety of applications discussed below.

**4.1. Heterogenous Catalysis.** *4.1.1. CO Oxidation.* Carbon monoxide oxidation is a regularly studied reaction to probe the efficiency of heterogeneous catalysts while also having environmental significance.[94] Cerium oxide has a fluorite structure and crystallizes into the cubic system and naturally forms the (111) facet. The surface energies are as follows (111) 0.69 J/m$^2$, (110) 1.04 J/m$^2$, and (100) 1.41 J/m$^2$.[37] By these surface energies, the (111) facet should not be chemically as active as its counterparts which was later validated by Wu et al. where CO oxidation was found to be enhanced and bonded more strongly on ceria reactive rods (110) and ceria cube (100) surfaces than on the less reactive octahedral surface (111).[38] However, more recently, $CeO_2$ (111) nanorods doped with palladium showed better catalytic performance than palladium supported on $CeO_2$ (100) cubes for CO oxidation.[13] This might be due to the recent discovery that ceria nanorods contain a few high-energy (100) facets and are actually enclosed by (111) facets and not (110) facets as previously claimed, so the high-energy (100) facets may be more likely contributing to the enhanced catalytic activity rather than the (111) facet.[13,95,96] To validate the facet enclosure of ceria nanorods, a recent study using infrared reflection absorption spectroscopy confirmed that the ceria rods are mainly enclosed by (111) facets.[13,97]

Cobalt oxide has a spinel structure and crystallizes into the cubic system with the (100) facet being the most stable. The surface energies are as follows: (100) 1.39 J/m$^2$, (111) 1.48 J/m$^2$, and (110) 1.65 J/m$^2$.[98] The plate-like nanocrystals of $Co_3O_4$ (111) that Teng et al. synthesized showed the highest catalytic activity toward CO oxidation compared to rods, cubes, and spheres not possessing the (111) facet.[16] The high catalytic activity was speculated to be due to the retention of active sites on the (111) facet when dry reactant gas streams are used.

Lanthanum based cobaltites have a perovskite structure and crystallize into the hexagonal crystal system, but at temperatures above 900 °C they transform into a cubic perovskite.[11,12] The most stable facet is the (100).[44] $LaCoO_3$ (111) and $La_{0.7}Sr_{0.3}CoO_3$ (111) in Wang et al.'s study showed enhanced catalytic activity for CO oxidations compared to its (110/100) counterpart.[6] Between both (111) faceted catalysts, $La_{0.7}Sr_{0.3}CoO_3$ (111) performed the best for CO oxidation. This was due to the finding that (111) facets contain more oxygen species and active cobalt ions compared to $LaCoO_3$ containing both (110) and (100) facets. Additionally, they found that the exposed high-energy (111) facet combined with strontium doping can improve the hybridization between cobalt cations and oxygen anions resulting in their oxygen p-band center being closer to the Fermi level, which also contributes to the higher catalytic activity.[6]

*4.1.2. Photocatalysis.* The process of photocatalysis involves a catalyst that is able to absorb light and convert it to use in a chemical reaction and has use in a variety of environmental applications such as wastewater remediation.[99]

The titanium dioxide described in this review as a case study has an anatase structure and crystallizes into the tetragonal system with the (101) facet being the most stable. The surface energies of facets in the anatase structure are as follows: (101) 0.44 J/m$^2$, (110) 1.09 J/m$^2$, and (111) 1.61 J/m$^2$.[40,41] Nanoscale anatase $TiO_2$ (111) synthesized by Zhang et al. showed improved photocatalytic activity toward the degradation of methylene blue (MB) and rhodamine B (RhB) dyes in aqueous solution, 2−3 times than that of $TiO_2$ nanosheets with exposed (001) facets and commercial Degussa P25 (101).[14] The authors attribute the enhanced photocatalytic activity to the (111) surface which contains unsaturated titanium and oxygen atoms which results in higher adsorption and degradation activity.[14]

Copper oxide has a cuprite structure and crystallizes into the cubic system with the (100) facet being the most stable.[44] Like $TiO_2$, cuprite (111) materials in both microcrystal and nanosphere morphology also have a higher photocatalytic degradation of the methyl orange dye compared to its (100) counterpart mainly due to the unsaturated copper cations on the (111) surface.[27,28]

Nickel oxide has a rock-salt structure and crystallizes into the cubic system with the (100) facet being the most stable.[9] Octahedral NiO (111) synthesized by Hermawan et al. exhibited the best $NO_x$ gas sensing response and photocatalytic degradation of $NO_x$ compared to the (110) facet for NiO.[24] The increased activity is due to the presence of nickel atoms on the


https://doi.org/10.1021/acs.cgd.2c00409
Cryst. Growth Des. 2022, 22, 6296−6322

clean (111) facet (Ni-terminated), and moreover surface areas were not a factor for increased activity.[24]

*4.1.3. Thermodecompostion.* Ammonium perchlorate (AP) is an oxidizer used in propellants, and achieving lower decomposition temperatures is an active research pursuit.[100] The catalytic activity characterization of $Co_3O_4$ (111) octahedra synthesized by Zhou et al. showed it could catalyze the thermal decomposition of ammonium perchlorate effectively by lowering the initial decomposition temperature by 137 °C.[17] The authors explain this by the (111) facet of $Co_3O_4$ possessing more $Co^{2+}$ which is beneficial to catalyze the ammonium perchlorate.

*4.1.4. Biomass Conversion.* Biomass catalytic conversion into higher valued products such as biofuels presents a research area with the capacity to change the environment for the better. Magnesium oxide has a rock-salt structure, crystallizes in the cubic system, and contains the (100) facet as its naturally occurring facet.[9] MgO (111) displayed enhanced catalytic activity during the transesterification reaction of sunflower and rapeseed oil to biodiesel compared to its counterpart facets.[46] In a different study, this same material also showed enhanced catalytic activity toward 2-pentanone condensation to biofuel precursor products compared to its counterpart facets.[48] Additionally, in the same study, when the catalyst is exposed to water, it experiences a reduction in activity and surface area; however, upon thermal regeneration treatment, activity and surface area are reestablished.[48] Overall, the reason for increased catalytic activity for MgO (111) boils down to its unique surface atomic arrangement consisting of monolayers of cations and anions with the surface being oxygen terminated making it a great Lewis-base catalyst.

*4.1.5. Claisen-Schmidt Condensation.* The Claisen-Schmidt condensation reaction results in a carbon−carbon bond formation and has various applications in pharmaceuticals and fine chemical industries.[1]

MgO (111) displayed improved catalytic activity in the Claisen-Schmidt condensation reaction of acetophenone and benzaldehyde compared to its counterpart facets and high surface area MgO in a facet other than (111).[20,101]

*4.1.6. Catalyst Support.* MgO(111) synthesized by Zhu et al. found use as a catalyst support due to its oxygen rich nature and intermediate basicity. Vanadium oxide supported on MgO(111) superseded that of conventional MgO in the (100) facet for the oxidative dehydrogenation of ethylbenzene with carbon dioxide.[19] Similarly, MgO(111) synthesized by Huang et al. served as a support material that enhanced the photocatalytic activity of g-$C_3N_4$ toward the degradation of methyl orange (MO) via a local electric field induced by MgO(111).[102]

**4.2. Adsorbent Materials.** MgO(111) synthesized by Mutch et al. revealed enhanced adsorptive properties toward carbon capturing compared to that of nanoscale and bulk MgO both having the (100) facet.[47] As previously stated, because the (111) surface contains an abundance of oxygen anions, it readily adsorbs carbon dioxide.

NiO(111) synthesized by Song et al. was shown to have an application as an efficient and recyclable adsorbent for the dye pollutant removal of brilliant red X-3B, Congo red, and fuchsin red compared to its counterpart facets.[103] The authors speculated the dye removal to be due to the (111) surface consisting of alternating monolayers of oxygen anions and nickel cations creating a strong electrostatic field perpendicular to the (111) surface resulting in an electrostatic interaction between the nickel oxide surface and the dye.[103]

**4.3. Energy Storage.** Energy storage in the forms of chemical, thermal, electric, or kinetic is a way to store energy with the goal to have it accessible upon demand, which is important toward the reliability and transition from fossil fuels to renewable energy technologies.[104] The atomically thin $Co_3O_4$ (111) nanosheets created by Zhu et al. exhibited enhanced lithium storage performance.[18] The increased storage can be attributed to the increased number of $Co^{2+}$ atoms and charge redistribution on the (111) faceted atomically thin nanosheets.[18]

**4.4. Antibacterial Materials.** MgO (111) synthesized by Hao et al. had great performance for reactive oxygen species generation in the dark for antibacterial application compared to its (100) facet counterpart.[22] The authors declared that the molecule transition and electron rearrangement process can occur only through a chemisorption interaction between the adsorbed $O_2$ and (111) facet-exposed MgO with abundant surface oxygen vacancies which produce singlet oxygen and superoxide anion radicals in the dark.[22]

## 5. CONCLUSIONS

The (111) facet for metal oxides of various crystal systems utilizing multiple synthetic methods has been reviewed. The overarching theme shown is that crystal facet exposure depends on the thermodynamic nature of the system. By default, a material will want to crystallize in the easiest way possible; in other words, it will crystallize into its most thermodynamically stable facet. The controlled exposure of the (111) facet on metal oxides relies on lowering the surface energy, which is accomplished with the aid of specific and critical synthetic parameters. There is still a research gap on concrete and definitive surface terminations of (111) faceted surfaces across metal oxides that are not well-known such as the example of $CeO_2$ (111) nanorods. One way to help mitigate this is by pursuing a combination of computation and surface sensitive characterization as well as the use of Tasker's surface categorization. Upcoming studies on faceted materials should therefore consider the surface energy primarily, understand the surface arrangement with confidence (e.g., Tasker surfaces, computational modeling, and reliable characterization), and utilize these methods to explore facet-dependent properties and even adapt synthesis to new metal oxides that have not yet been synthesized in the (111) facet orientation such as calcium oxide (CaO).

## AUTHOR INFORMATION


### Corresponding Author

**Ryan M. Richards** − *Department of Chemistry, Colorado School of Mines, Golden, Colorado 80401, United States; National Renewable Energy Laboratory, Golden, Colorado 80401, United States;* orcid.org/0000-0001-8792-3964; Email: rrichard@mines.edu

### Authors

**Raiven I. Balderas** − *Department of Chemistry, Colorado School of Mines, Golden, Colorado 80401, United States; National Renewable Energy Laboratory, Golden, Colorado 80401, United States;* orcid.org/0000-0002-2659-675X

**Cristian V. Ciobanu** − *Department of Mechanical Engineering, Colorado School of Mines, Golden, Colorado 80401, United States; National Renewable Energy Laboratory, Golden, Colorado 80401, United States;* orcid.org/0000-0002-8476-4467




https://doi.org/10.1021/acs.cgd.2c00409
Cryst. Growth Des. 2022, 22, 6296−6322

Complete contact information is available at:
https://pubs.acs.org/10.1021/acs.cgd.2c00409

## Notes

The authors declare no competing financial interest.

## Biographies

Raiven I. Balderas is a fourth year Ph.D. candidate in the applied chemistry program at Colorado School of Mines. She received her ACS certified B.Sc. degree in chemistry from The University of Texas Rio Grande Valley in 2019 and also completed two minors in applied mathematics and statistics. Currently, her research involves the synthesis and characterization of faceted metal oxides for renewable energy applications. She conducts a large portion of her research at the National Renewable Energy Laboratory where she tests various catalysts for the hydrodeoxygenation of biomass-derived ketones into sustainable aviation fuels. Raiven has also mentored various undergraduates and has presented her research at various conferences. Recently, she won second place in student oral presentations at the 2022 Rocky Mountain Catalysis Society Symposium.

Dr. Cristian V. Ciobanu is a professor in the Department of Mechanical Engineering and in the Materials Science Program at Colorado School of Mines, as well as a joint appointee at the National Renewable Energy Laboratory (NREL). Prof. Ciobanu received his B.S. in physics from University of Bucharest, and his M.S. and Ph.D. in physics from The Ohio State University. He joined Mines in 2004 after a postdoctoral stage at Brown University. Prof. Ciobanu has more than 100 publications with about 4000 citations, 2 patents, and 1 authored book in the areas of crystal and surface structure, optimization algorithms, 2D materials, nanomaterials, and structure−property relationships. Prof. Ciobanu serves in several of professional societies and is a Fellow of the Royal Society of Chemistry and a Fellow of the Institute of Physics.

Dr. Ryan M. Richards is a professor of chemistry and materials science with a joint appointment at the National Renewable Energy Laboratory (NREL) both in Golden, Colorado USA. Prof. Richards is also co-lead of the Mines/NREL Nexus at the Colorado School of Mines. Ryan received his B.S. from Michigan State University, M.S. from Central Michigan University, and Ph.D. from Kansas State University. He has been a visiting scientist at the Boreskov Institute of Catalysis in Novosibirsk, Russia, and a postdoctoral fellow at the Max Planck Institute für Kohlenforschung in Germany. His independent career started as an assistant professor at Jacobs University Bremen (Germany), and in 2007 he moved to the Colorado School of Mines and NREL where he was promoted to Professor in 2012. Prof. Richards has more than 160 publications, >10,000 citations, 7 patents, and 3 edited books in the areas of green chemistry, renewable energy, sustainability, catalysis and nanomaterials. Further, Prof. Richards has been selected by his peers for a number of prestigious awards including as a Fellow of the American Chemical Society.

## ■ ACKNOWLEDGMENTS

R.I.B. and R.M.R. acknowledge DOE Contract No. DE-AC36-08GO28308. Additionally, R.M.R. acknowledges NSF CBET Grant No. 2139971 for support.

## ■ REFERENCES

(1) Cadigan, C. A.; Corpuz, A. R.; Lin, F.; Caskey, C. M.; Finch, K. B. H.; Wang, X.; Richards, R. M. Nanoscale (111) faceted rock-salt metal oxides in catalysis. *Catalysis Science & Technology* **2013**, *3* (4), 900−911.
(2) Pal, J.; Pal, T. Faceted metal and metal oxide nanoparticles: design, fabrication and catalysis. *Nanoscale* **2015**, *7* (34), 14159−14190.
(3) Zhao, X. H.; Susman, M. D.; Rimer, J. D.; Bollini, P. Synthesis, Structure and Catalytic Properties of Faceted Oxide Crystals. *ChemCatChem.* **2021**, *13* (1), 6−27.
(4) Sun, S. D.; Zhang, X.; Cui, J.; Yang, Q.; Liang, S. H. High-index faceted metal oxide micro-/nanostructures: a review on their characterization, synthesis and applications. *Nanoscale* **2019**, *11* (34), 15739−15762.
(5) Xu, T.; Zhou, X.; Jiang, Z. Y.; Kuang, Q.; Xie, Z. X.; Zheng, L. S. Syntheses of Nano/Submicrostructured Metal Oxides with All Polar Surfaces Exposed via a Molten Salt Route. *Cryst. Growth Des.* **2009**, *9* (1), 192−196.
(6) Wang, X. Y.; Huang, K. K.; Yuan, L.; Li, S.; Ma, W.; Liu, Z. Y.; Feng, S. H. Molten Salt Flux Synthesis, Crystal Facet Design, Characterization, Electronic Structure, and Catalytic Properties of Perovskite Cobaltite. *ACS Appl. Mater. Interfaces* **2018**, *10* (33), 28219−28231.
(7) Kuang, Q.; Wang, X.; Jiang, Z. Y.; Xie, Z. X.; Zheng, L. S. High-Energy-Surface Engineered Metal Oxide Micro- and Nanocrystallites and Their Applications. *Acc. Chem. Res.* **2014**, *47* (2), 308−318.

(8) Susman, M. D.; Pham, H. N.; Datye, A. K.; Chinta, S.; Rimer, J. D. Factors Governing MgO(111) Faceting in the Thermal Decomposition of Oxide Precursors. *Chem. Mater.* **2018**, *30* (8), 2641−2650.
(9) Sterrer, M.; Freund, H.-J. Properties of Oxide Surfaces. *Surface and Interface Science* **2013**, 229−278.
(10) Johnsson, M.; Lemmens, P. Perovskites and thin films - crystallography and chemistry. *J. Phys.: Condens. Matter* **2008**, *20* (26), 64001.
(11) Buckeridge, J.; Taylor, F. H.; Catlow, C. R. A. Efficient and accurate approach to modeling the microstructure and defect properties of $LaCoO_3$. *Phys. Rev. B* **2016**, *93* (15), 155123.
(12) van Doorn, R. H. E.; Burggraaf, A. J. Structural aspects of the ionic conductivity of La1-xSrxCoO3-delta. *Solid State Ionics* **2000**, *128* (1−4), 65−78.
(13) Spezzati, G.; Benavidez, A. D.; DeLaRiva, A. T.; Su, Y. Q.; Hofmann, J. P.; Asahina, S.; Olivier, E. J.; Neethling, J. H.; Miller, J. T.; Datye, A. K.; Hensen, E. J. M. CO oxidation by Pd supported on CeO2(100) and CeO2(111) facets. *Appl. Catal., B* **2019**, *243*, 36−46.
(14) Zhang, J.; Qian, L. S.; Yang, L. X.; Tao, X.; Su, K. P.; Wang, H. B.; Xi, J. H.; Ji, Z. G. Nanoscale anatase $TiO_2$ with dominant {111} facets shows high photocatalytic activity. *Appl. Surf. Sci.* **2014**, *311*, 521−528.
(15) Grybos, J.; Hudy, C.; Gryczynska, A.; Piskorz, W.; Sojka, Z. Hydrothermal Synthesis of Euhedral $Co_3O_4$ Nanocrystals via Nutrient-Assisted Topotactic Transformation of the Layered Co(OH)(2) Precursor under Anoxic Conditions: Insights into Intricate Routes Leading to Spinel Phase Development and Shape Perfection. *Cryst. Growth Des.* **2020**, *20* (12), 7771−7787.
(16) Teng, Y. H.; Kusano, Y.; Azuma, M.; Haruta, M.; Shimakawa, Y. Morphology effects of $Co_3O_4$ nanocrystals catalyzing CO oxidation in a dry reactant gas stream. *Catalysis Science & Technology* **2011**, *1* (6), 920−922.
(17) Zhou, H.; Lv, B. L.; Wu, D.; Xu, Y. Synthesis and properties of octahedral $Co_3O_4$ single-crystalline nanoparticles enclosed by (111) facets. *CrystEngComm* **2013**, *15* (41), 8337−8344.
(18) Zhu, J. B.; Bai, L. F.; Sun, Y. F.; Zhang, X. D.; Li, Q. Y.; Cao, B. X.; Yan, W. S.; Xie, Y. Topochemical transformation route to atomically thick Co3O4 nanosheets realizing enhanced lithium storage performance. *Nanoscale* **2013**, *5* (12), 5241−5246.
(19) Zhu, K. K.; Hua, W. M.; Deng, W.; Richards, R. M. Preparation of MgO Nanosheets with Polar (111) Surfaces by Ligand Exchange and Esterification - Synthesis, Structure, and Application as Catalyst Support. *Eur. J. Inorg. Chem.* **2012**, *2012* (17), 2869−2876.
(20) Zhu, K. K.; Hu, J. C.; Kubel, C.; Richards, R. Efficient preparation and catalytic activity of MgO(111) nanosheets. *Angew. Chem., Int. Ed.* **2006**, *45* (43), 7277−7281.
(21) Liu, P. X.; Abdala, P. M.; Goubert, G.; Willinger, M. G.; Coperet, C. Ultrathin Single Crystalline MgO(111) Nanosheets. *Angew. Chem., Int. Ed.* **2021**, *60* (6), 3254−3260.
(22) Hao, Y. J.; Liu, B.; Tian, L. G.; Li, F. T.; Ren, J.; Liu, S. J.; Liu, Y.; Zhao, J.; Wang, X. J. Synthesis of {111} Facet-Exposed MgO with Surface Oxygen Vacancies for Reactive Oxygen Species Generation in the Dark. *ACS Appl. Mater. Interfaces* **2017**, *9* (14), 12687−12693.
(23) Hu, J. C.; Zhu, K. K.; Chen, L. F.; Yang, H. J.; Li, Z.; Suchopar, A.; Richards, R. Preparation and surface activity of single-crystalline NiO(111) nanosheets with hexagonal holes: A semiconductor nanospanner. *Adv. Mater.* **2008**, *20* (2), 267.
(24) Hermawan, A.; Hanindriyo, A. T.; Ramadhan, E. R.; Asakura, Y.; Hasegawa, T.; Hongo, K.; Inada, M.; Maezono, R.; Yin, S. Octahedral morphology of NiO with (111) facet synthesized from the transformation of NiOHCl for the NOx detection and degradation: experiment and DFT calculation. *Inorganic Chemistry Frontiers* **2020**, *7* (18), 3431−3442.
(25) Susman, M. D.; Pham, H. N.; Zhao, X. H.; West, D. H.; Chinta, S.; Bollini, P.; Datye, A. K.; Rimer, J. D. Synthesis of NiO Crystals Exposing Stable High-Index Facets. *Angew. Chem., Int. Ed.* **2020**, *59* (35), 15119−15123.
(26) Zhou, Z. J.; Zhu, X. L.; Wu, D. J.; Chen, Q. L.; Huang, D. T.; Sun, C. J.; Xin, J. Y.; Ni, K. Y.; Gao, J. H. Anisotropic Shaped Iron Oxide Nanostructures: Controlled Synthesis and Proton Relaxation Shortening Effects. *Chem. Mater.* **2015**, *27* (9), 3505−3515.
(27) Sun, S. D.; Zhang, X. Z.; Song, X. P.; Liang, S. H.; Wang, L. Q.; Yang, Z. M. Bottom-up assembly of hierarchical Cu2O nanospheres: controllable synthesis, formation mechanism and enhanced photochemical activities. *CrystEngComm* **2012**, *14* (10), 3545−3553.
(28) Li, A. L.; Li, P. W.; Hu, J.; Zhang, W. D. Crystal-facet-controllable synthesis of Cu2O microcrystals, shape evolution and their comparative photocatalytic activity. *Journal of Materials Science-Materials in Electronics* **2015**, *26* (7), 5071−5077.
(29) Likith, S. R. J.; Farberow, C. A.; Manna, S.; Abdulslam, A.; Stevanovic, V.; Ruddy, D. A.; Schaidle, J. A.; Robichaud, D. J.; Ciobanu, C. V. Thermodynamic Stability of Molybdenum Oxycarbides Formed from Orthorhombic Mo2C in Oxygen-Rich Environments. *J. Phys. Chem. C* **2018**, *122* (2), 1223−1233.
(30) Pimpinelli, A. The Equilibrium Crystal Shape. In *Physics of Crystal Growth*; Cambridge University Press: Collection Alea-Saclay: Monographs and Texts in Statistical Physics: Cambridge, 1998; pp 43−59.
(31) Pimpinelli, A. Growth and dissolution crystal shapes: Frank's model. In *Physics of Crystal Growth*; Cambridge University Press: Collection Alea-Saclay: Monographs and Texts in Statistical Physics: Cambridge, 1998; pp 60−69.
(32) Leong, G. J.; Ebnonnasir, A.; Schulze, M. C.; Strand, M. B.; Ngo, C.; Maloney, D.; Frisco, S. L.; Dinh, H. N.; Pivovar, B.; Gilmer, G. H.; Kodambaka, S.; Ciobanu, C. V.; Richards, R. M. Shape-directional growth of Pt and Pd nanoparticles. *Nanoscale* **2014**, *6* (19), 11364−11371.
(33) Kappes, B. B.; Leong, G. J.; Gilmer, G. H.; Richards, R. M.; Ciobanu, C. V. Metallic nanocrystals synthesized in solution: a brief review of crystal shape theory and crystallographic characterization. *Crystal Research and Technology* **2015**, *50* (9−10), 801−816.
(34) Ciobanu, C. V.; Ho, K.-M.; Wang, C.-Z. *Atomic Structure Prediction of Nanostructures, Clusters and Surfaces*, 1st ed.; Wiley-VCH: 2013; p 230.
(35) Ciobanu, C. V.; Predescu, C. Reconstruction of silicon surfaces: A stochastic optimization problem. *Phys. Rev. B* **2004**, *70* (8).
(36) Chuang, F. C.; Ciobanu, C. V.; Shenoy, V. B.; Wang, C. Z.; Ho, K. M. Finding the reconstructions of semiconductor surfaces via a genetic algorithm. *Surf. Sci.* **2004**, *573* (2), L375−L381.
(37) Nolan, M.; Parker, S. C.; Watson, G. W. The electronic structure of oxygen vacancy defects at the low index surfaces of ceria. *Surf. Sci.* **2005**, *595* (1−3), 223−232.
(38) Wu, Z. L.; Li, M. J.; Overbury, S. H. On the structure dependence of CO oxidation over CeO2 nanocrystals with well-defined surface planes. *J. Catal.* **2012**, *285* (1), 61−73.
(39) Conesa, J. C. Computer Modeling of Surfaces and Defects on Cerium Dioxide. *Surf. Sci.* **1995**, *339* (3), 337−352.
(40) Katal, R.; Masudy-Panah, S.; Tanhaei, M.; Farahani, M. H. D. A.; Jiangyong, H. A review on the synthesis of the various types of anatase TiO2 facets and their applications for photocatalysis. *Chemical Engineering Journal* **2020**, *384*, 123384.
(41) Diebold, U. The surface science of titanium dioxide. *Surf. Sci. Rep.* **2003**, *48* (5−8), 53−229.
(42) Davies, M. J.; Parker, S. C.; Watson, G. W. Atomistic Simulation of the Surface-Structure of Spinel. *J. Mater. Chem.* **1994**, *4* (6), 813−816.
(43) Kovalenko, M. V.; Bodnarchuk, M. I.; Lechner, R. T.; Hesser, G.; Schaffler, F.; Heiss, W. Fatty acid salts as stabilizers in size- and shape-controlled nanocrystal synthesis: The case of inverse spinel iron oxide. *J. Am. Chem. Soc.* **2007**, *129* (20), 6352.
(44) Huang, K. K.; Yuan, L.; Feng, S. H. Crystal facet tailoring arts in perovskite oxides. *Inorganic Chemistry Frontiers* **2015**, *2* (11), 965−981.
(45) Leng, M.; Liu, M. Z.; Zhang, Y. B.; Wang, Z. Q.; Yu, C.; Yang, X. G.; Zhang, H. J.; Wang, C. Polyhedral 50-Facet Cu2O Microcrystals Partially Enclosed by {311} High-Index Planes: Synthesis and Enhanced Catalytic CO Oxidation Activity. *J. Am. Chem. Soc.* **2010**, *132* (48), 17084−17087.


https://doi.org/10.1021/acs.cgd.2c00409
Cryst. Growth Des. 2022, 22, 6296−6322

(46) Verziu, M.; Cojocaru, B.; Hu, J. C.; Richards, R.; Ciuculescu, C.; Filip, P.; Parvulescu, V. I. Sunflower and rapeseed oil transesterification to biodiesel over different nanocrystalline MgO catalysts. *Green Chem.* **2008**, *10* (4), 373−381.
(47) Mutch, G. A.; Shulda, S.; McCue, A. J.; Menart, M. J.; Ciobanu, C. V.; Ngo, C.; Anderson, J. A.; Richards, R. M.; Vega-Maza, D. Carbon Capture by Metal Oxides: Unleashing the Potential of the (111) Facet. *J. Am. Chem. Soc.* **2018**, *140* (13), 4736−4742.
(48) Huo, X.; Conklin, D. R.; Zhou, M.; Vorotnikov, V.; Assary, R. S.; Purdy, S. C.; Page, K.; Li, Z.; Unocic, K. A.; Balderas, R. I.; Richards, R. M.; Vardon, D. R. Catalytic activity and water stability of the MgO(111) surface for 2-pentanone condensation. *Applied Catalysis B: Environmental* **2021**, *294*, 120234.
(49) Sun, T.; Wang, D. C.; Mirkin, M. V.; Cheng, H.; Zheng, J. C.; Richards, R. M.; Lin, F.; Xin, H. L. L. Direct high-resolution mapping of electrocatalytic activity of semi-two-dimensional catalysts with single-edge sensitivity. *Proc. Natl. Acad. Sci. U.S.A.* **2019**, *116* (24), 11618−11623.
(50) Thomele, D.; Baumann, S. O.; Schneider, J.; Sternig, A. K.; Shulda, S.; Richards, R. M.; Schwab, T.; Zickler, G. A.; Bourret, G. R.; Diwald, O. Cubes to Cubes: Organization of MgO Particles into One-Dimensional and Two-Dimensional Nanostructures. *Cryst. Growth Des.* **2021**, *21*, 4674.
(51) Tasker, P. W. Stability of Ionic-Crystal Surfaces. *Journal of Physics C-Solid State Physics* **1979**, *12* (22), 4977−4984.
(52) Hinuma, Y.; Kumagai, Y.; Oba, F.; Tanaka, I. Categorization of surface polarity from a crystallographic approach. *Comput. Mater. Sci.* **2016**, *113*, 221−230.
(53) Mullins, D. R. The surface chemistry of cerium oxide. *Surf. Sci. Rep.* **2015**, *70* (1), 42−85.
(54) Arita, R.; Tanida, Y.; Entani, S.; Kiguchi, M.; Saiki, K.; Aoki, H. Polar surface engineering in ultrathin MgO(111)/Ag(111): Possibility of a metal-insulator transition and magnetism. *Phys. Rev. B* **2004**, *69* (23), 235423.
(55) Wander, A.; Bush, I. J.; Harrison, N. M. Stability of rocksalt polar surfaces: An ab initio study of MgO(111) and NiO(111). *Phys. Rev. B* **2003**, *68* (23), 233405.
(56) Cappus, D.; Hassel, M.; Neuhaus, E.; Heber, M.; Rohr, F.; Freund, H. J. Polar Surfaces of Oxides - Reactivity and Reconstruction. *Surf. Sci.* **1995**, *337* (3), 268−277.
(57) Erdman, N.; Warschkow, O.; Ellis, D. E.; Marks, L. D. Solution of the p(2 × 2) NiO(111) surface structure using direct methods. *Surf. Sci.* **2000**, *470* (1−2), 1−14.
(58) Marks, L. D.; Chiaramonti, A. N.; Tran, F.; Blaha, P. The small unit cell reconstructions of SrTiO3(111). *Surf. Sci.* **2009**, *603* (14), 2179−2187.
(59) Plass, R.; Egan, K.; Collazo-Davila, C.; Grozea, D.; Landree, E.; Marks, L. D.; Gajdardziska-Josifovska, M. Cyclic ozone identified in magnesium oxide (111) surface reconstructions. *Phys. Rev. Lett.* **1998**, *81* (22), 4891−4894.
(60) Rohr, F.; Wirth, K.; Libuda, J.; Cappus, D.; Baumer, M.; Freund, H. J. Hydroxyl Driven Reconstruction of the Polar NIO(111) Surface. *Surf. Sci.* **1994**, *315* (1−2), L977−L982.
(61) Wang, Z. L.; Feng, X. D. Polyhedral shapes of $CeO_2$ nanoparticles. *J. Phys. Chem. B* **2003**, *107* (49), 13563−13566.
(62) Zhou, K. B.; Wang, X.; Sun, X. M.; Peng, Q.; Li, Y. D. Enhanced catalytic activity of ceria nanorods from well-defined reactive crystal planes. *J. Catal.* **2005**, *229* (1), 206−212.
(63) Mai, H. X.; Sun, L. D.; Zhang, Y. W.; Si, R.; Feng, W.; Zhang, H. P.; Liu, H. C.; Yan, C. H. Shape-selective synthesis and oxygen storage behavior of ceria nanopolyhedra, nanorods, and nanocubes. *J. Phys. Chem. B* **2005**, *109* (51), 24380−24385.
(64) Li, W. J.; Shi, E. W.; Zhong, W. Z.; Yin, Z. W. Growth mechanism and growth habit of oxide crystals. *J. Cryst. Growth* **1999**, *203* (1−2), 186−196.
(65) Zhu, Y. Z.; Takami, S.; Seong, G. Y.; Dejhosseini, M.; Hossain, M. Z.; Noguchi, T.; Hojo, D.; Aoki, N.; Aida, T.; Adschiri, T. Green solvent for green materials: a supercritical hydrothermal method and shape-controlled synthesis of Cr-doped $CeO_2$ nanoparticles. *Philosophical Transactions of the Royal Society a-Mathematical Physical and Engineering Sciences* **2015**, *373* (2057), 20150012.
(66) Cushing, B. L.; Kolesnichenko, V. L.; O'Connor, C. J. Recent advances in the liquid-phase syntheses of inorganic nanoparticles. *Chem. Rev.* **2004**, *104* (9), 3893−3946.
(67) AZoNano. Colbalt Oxide ($Co_3O_4$) Nanoparticles - Properties, Applications 2013. https://www.azonano.com/article.aspx?ArticleID=3387.
(68) Hermawan, A.; Asakura, Y.; Inada, M.; Yin, S. One-step synthesis of micro-/mesoporous $SnO_2$ spheres by solvothermal method for toluene gas sensor. *Ceram. Int.* **2019**, *45* (12), 15435−15444.
(69) Guo, C. S.; Wu, X. Y.; Yan, M.; Dong, Q.; Yin, S.; Sato, T.; Liu, S. Q. The visible-light driven photocatalytic destruction of NOx using mesoporous $TiO_2$ spheres synthesized via a "water-controlled release process". *Nanoscale* **2013**, *5* (17), 8184−8191.
(70) Ivanda, M.; Music, S.; Popovic, S.; Gotic, M. XRD, Raman and FT-IR spectroscopic observations of nanosized $TiO_2$ synthesized by the sol-gel method based on an esterification reaction. *J. Mol. Struct.* **1999**, *481*, 645−649.
(71) Styskalik, A.; Skoda, D.; Barnes, C. E.; Pinkas, J. The Power of Non-Hydrolytic Sol-Gel Chemistry: A Review. *Catalysts* **2017**, *7* (6), 168.
(72) Taubert, A.; Li, Z. Inorganic materials from ionic liquids. *Dalton Transactions* **2007**, No. 7, 723−727.
(73) Morris, R. E. Ionothermal synthesis-ionic liquids as functional solvents in the preparation of crystalline materials. *Chem. Commun.* **2009**, No. 21, 2990−2998.
(74) Ahmed, E.; Breternitz, J.; Groh, M. F.; Ruck, M. Ionic liquids as crystallisation media for inorganic materials. *CrystEngComm* **2012**, *14* (15), 4874−4885.
(75) Zhang, H.; Dasbiswas, K.; Ludwig, N. B.; Han, G.; Lee, B.; Vaikuntanathan, S.; Talapin, D. V. Stable colloids in molten inorganic salts. *Nature* **2017**, *542* (7641), 328.
(76) Cornell, R. M.; Schertmann, U. *The Iron Oxides: Structure, Properties, Reactions, Occurrences and Uses*; Wiley: New York, 1996.
(77) Gao, J. H.; Gu, H. W.; Xu, B. Multifunctional Magnetic Nanoparticles: Design, Synthesis, and Biomedical Applications. *Acc. Chem. Res.* **2009**, *42* (8), 1097−1107.
(78) Jagadeesh, R. V.; Surkus, A. E.; Junge, H.; Pohl, M. M.; Radnik, J.; Rabeah, J.; Huan, H. M.; Schunemann, V.; Bruckner, A.; Beller, M. Nanoscale Fe2O3-Based Catalysts for Selective Hydrogenation of Nitroarenes to Anilines. *Science* **2013**, *342* (6162), 1073−1076.
(79) Laurent, S.; Forge, D.; Port, M.; Roch, A.; Robic, C.; Vander Elst, L.; Muller, R. N. Magnetic iron oxide nanoparticles: Synthesis, stabilization, vectorization, physicochemical characterizations, and biological applications. *Chem. Rev.* **2008**, *108* (6), 2064−2110.
(80) Reddy, L. H.; Arias, J. L.; Nicolas, J.; Couvreur, P. Magnetic Nanoparticles: Design and Characterization, Toxicity and Biocompatibility, Pharmaceutical and Biomedical Applications. *Chem. Rev.* **2012**, *112* (11), 5818−5878.
(81) Teng, X. W.; Black, D.; Watkins, N. J.; Gao, Y. L.; Yang, H. Platinum-maghemite core-shell nanoparticles using a sequential synthesis. *Nano Lett.* **2003**, *3* (2), 261−264.
(82) Zhou, K.; Li, Y. Catalysis Based on Nanocrystals with Well-Defined Facets. *Angew. Chem., Int. Ed* **2012**, *51*, 602−613.
(83) Zeng, H.; Li, J.; Liu, J. P.; Wang, Z. L.; Sun, S. H. Exchange-coupled nanocomposite magnets by nanoparticle self-assembly. *Nature* **2002**, *420* (6914), 395−398.
(84) Su, D. W.; Horvat, J.; Munroe, P.; Ahn, H.; Ranjbartoreh, A. R.; Wang, G. X. Polyhedral Magnetite Nanocrystals with Multiple Facets: Facile Synthesis, Structural Modelling, Magnetic Properties and Application for High Capacity Lithium Storage. *Chem.—Eur. J.* **2012**, *18* (2), 488−497.
(85) Zhou, X.; Xie, Z. X.; Jiang, Z. Y.; Kuang, Q.; Zhang, S. H.; Xu, T.; Huang, R. B.; Zheng, L. S. Formation of ZnO hexagonal micro-pyramids: a successful control of the exposed polar surfaces with the assistance of an ionic liquid. *Chem. Commun.* **2005**, No. 44, 5572−5574.
(86) Estelle, J.; Salagre, P.; Cesteros, Y.; Serra, M.; Medina, F.; Sueiras, J. E. Comparative study of the morphology and surface properties of


https://doi.org/10.1021/acs.cgd.2c00409
*Cryst. Growth Des.* 2022, 22, 6296−6322

nickel oxide prepared from different precursors. *Solid State Ionics* **2003**, *156* (1−2), 233−243.
(87) Lou, X. W.; Deng, D.; Lee, J. Y.; Feng, J.; Archer, L. A. Self-supported formatnion of needlelike Co3O4 nanotubes and their application as lithium-ion battery electrodes. *Adv. Mater.* **2008**, *20* (2), 258.
(88) Tian, L.; Zou, H. L.; Fu, J. X.; Yang, X. F.; Wang, Y.; Guo, H. L.; Fu, X. H.; Liang, C. L.; Wu, M. M.; Shen, P. K.; Gao, Q. M. Topotactic Conversion Route to Mesoporous Quasi-Single-Crystalline Co3O4 Nanobelts with Optimizable Electrochemical Performance. *Adv. Funct. Mater.* **2010**, *20* (4), 617−623.
(89) Tan, C. L.; Zhang, H. Wet-chemical synthesis and applications of non-layer structured two-dimensional nanomaterials. *Nat. Commun.* **2015**, *6*, 7873.
(90) Dou, Y. H.; Zhang, L.; Xu, X.; Sun, Z. Q.; Liao, T.; Dou, S. X. Atomically thin non-layered nanomaterials for energy storage and conversion. *Chem. Soc. Rev.* **2017**, *46* (23), 7338−7373.
(91) Lei, F. C.; Sun, Y. F.; Liu, K. T.; Gao, S.; Liang, L.; Pan, B. C.; Xie, Y. Oxygen Vacancies Confined in Ultrathin Indium Oxide Porous Sheets for Promoted Visible-Light Water Splitting. *J. Am. Chem. Soc.* **2014**, *136* (19), 6826−6829.
(92) Kuang, Y.; Feng, G.; Li, P. S.; Bi, Y. M.; Li, Y. P.; Sun, X. M. Single-Crystalline Ultrathin Nickel Nanosheets Array from In Situ Topotactic Reduction for Active and Stable Electrocatalysis. *Angew. Chem., Int. Ed.* **2016**, *55* (2), 693−697.
(93) Varma, A.; Mukasyan, A. S.; Rogachev, A. S.; Manukyan, K. V. Solution Combustion Synthesis of Nanoscale Materials. *Chem. Rev.* **2016**, *116* (23), 14493−14586.
(94) Zhou, Y.; Wang, Z. Y.; Liu, C. J. Perspective on CO oxidation over Pd-based catalysts. *Catalysis Science & Technology* **2015**, *5* (1), 69−81.
(95) Agarwal, S.; Lefferts, L.; Mojet, B. L.; Ligthart, D.; Hensen, E. J. M.; Mitchell, D. R. G.; Erasmus, W. J.; Anderson, B. G.; Olivier, E. J.; Neethling, J. H.; Datye, A. K. Exposed Surfaces on Shape-Controlled Ceria Nanoparticles Revealed through AC-TEM and Water-Gas Shift Reactivity. *ChemSusChem* **2013**, *6* (10), 1898−1906.
(96) Ji, Z.; Wang, X.; Zhang, H.; Lin, S.; Meng, H.; Sun, B.; George, S.; Xia, T.; Nel, A. E.; Zink, J. I. Designed Synthesis of CeO2 Nanorods and Nanowires for Studying Toxicological Effects of High Aspect Ratio Nanomaterials. *ACS Nano* **2012**, *6* (6), 5366−5380.
(97) Yang, C. W.; Yu, X. J.; Heissler, S.; Nefedov, A.; Colussi, S.; Llorca, J.; Trovarelli, A.; Wang, Y. M.; Woll, C. Surface Faceting and Reconstruction of Ceria Nanoparticles. *Angew. Chem., Int. Ed.* **2017**, *56* (1), 375−379.
(98) Sun, H. Q.; Ang, H. M.; Tade, M. O.; Wang, S. B. Co3O4 nanocrystals with predominantly exposed facets: synthesis, environmental and energy applications. *Journal of Materials Chemistry A* **2013**, *1* (46), 14427−14442.
(99) El Nazer, H. E. A. F. A. H.; Gaballah, S. T. Nanocomposites and Its Importance in Photocatalysis. In *Nanocomposites for Visible Light-induced Photocatalysis*; Springer, 2017; pp 41−67.
(100) Wang, Y.; Song, X. L.; Li, F. S. Thermal Behavior and Decomposition Mechanism of Ammonium Perchlorate and Ammonium Nitrate in the Presence of Nanometer Triaminoguanidine Nitrate. *Acs Omega* **2019**, *4* (1), 214−225.
(101) Choudary, B. M.; Kantam, M. L.; Ranganath, K. V. S.; Mahendar, K.; Sreedhar, B. Bifunctional nanocrystalline MgO for chiral epoxy ketones via Claisen-Schmidt condensation-asymmetric epoxidation reactions. *J. Am. Chem. Soc.* **2004**, *126* (11), 3396−3397.
(102) Huang, Z.; Zhao, X.; Xia, H.; Lu, F.; Hu, L.; Chu, P. K. Insights into Enhancement of Photocatalytic Properties of g-$C_3N_4$ by Local Electric Field Induced by Polarization of MgO(111). *Journal of Environmental Chemical Engineering* **2021**, *9*, 105922 DOI: 10.1016/j.jece.2021.105922.
(103) Song, Z.; Chen, L. F.; Hu, J. C.; Richards, R. M. NiO(111) nanosheets as adsorbents for dye pollutants removal from wastewater. *Abstracts of Papers of the American Chemical Society* **2009**, *237*.
(104) Revankar, S. T. Chemical Energy Storage. In *Storage and Hybridization of Nuclear Energy*; Elsevier, 2019; pp 177−227.




https://doi.org/10.1021/acs.cgd.2c00409
*Cryst. Growth Des.* 2022, 22, 6296−6322